



NICHOLAS SCHOOL OF THE ENVIRONMENT
DUKE UNIVERSITY

DIVISION OF EARTH & OCEAN SCIENCES

Wednesday, September 13, 2017

Jack Middelburg
Editor
Biogeosciences

Dear Dr. Middelburg,

We would first like to thank you and the three reviewers for the careful examination of our manuscript and the insightful comments. We have taken into account these comments in the revised manuscript.

Below is a response to the reviewers' comments and the revised manuscript. Please do not hesitate to contact us should you have any additional questions or comments on our manuscript.

Sincerely,
Zuchuan Li

Division of Earth and Ocean Sciences
Nicholas School of the Environment
Duke University
email. zuchuan.li@duke.edu



Reviewer 1:

We thank the reviewer for his/her review of our manuscript. We disagree with his/her overall assessment. Below, we provide a response to the reviewer's two points:

- The reviewer's first comment states that our results "... show that this maximum constraint is consistent with past estimates of carbon export. As such, the analysis seems incomplete in failing to describe what new insight the current theoretical constraint provides"

As stated in the manuscript, our impetus for this study is to explain the recently reported field observations of an interesting relationship between export production proxies and mixed layer depths (Cassar et al., 2011; Eveleth et al., 2017; Tortell et al., 2015). Our theoretical considerations build on the qualitative description provided in these original studies.

We now further emphasize the key outcomes of our study in the introduction section of the manuscript, and enumerate them here: 1) the development of a mechanistic model of an upper bound on carbon export based on the metabolic balance of photosynthesis and respiration in the oceanic mixed layer, 2) using parameters available in the literature, the modeled upper bound envelopes field observations of export production estimated from ^{234}Th and sediment traps and O_2/Ar -derived net community production, and 3) the model identifies regions of the Southern Ocean where carbon export is likely limited by light during part of the growing season. Our effort has significant implications for unraveling the influence of light and nutrients availability on carbon export production in the surface ocean (see Figure 5 of the revised manuscript), and for the development of models of export production based on satellite dataproducts.

Numerous recent modeling efforts have used simplified models to explore patterns in field observations. As an example, we refer the reviewer to the recent study of Cael and Follows (2016). In their study, the authors elegantly use "what is arguably the simplest mechanistic model" to explain the observed dependence of carbon export efficiency on temperature.

- The reviewer's second comment, related to the first, states that "...the mathematical posing an equation for maximum possible export includes extremely simplified assumptions such as first-order herbivory that is constant with depth..."

We, again, refer the reviewer to the multitude of recent modelling efforts which have used simplified equations for complex biogeochemical processes, including herbivory. Many recent studies use first-order kinetics for grazing losses and other assumptions (e.g., see Equation 1 in Cael and Follows, 2016; Cael et al., 2017; Dutkiewicz et al., 2001; Gong et al., 2015; Gong et al., 2017; Huisman et al., 2006; Taylor and Ferrari, 2011).

Most (if not all) of these recent studies also assume constant herbivory and biogeochemical properties with depth within the mixed layer (Cael and Follows, 2016; Cael et al., 2017; Dutkiewicz et al., 2001; Gong et al., 2015; Gong et al., 2017; Huisman et al., 2006; Siegel et al., 2014; Taylor and Ferrari, 2011). Nonetheless, we now further describe in the manuscript the limitations associated with Sverdrup's assumption of homogeneously mixed organisms or constant loss rates with depth within the mixed layer.

Overall, the reviewer's comments are unfounded in light of the fact that 1) many other *recently* published articles have used similar modeling approaches and equations, and 2) to the best of our knowledge, this is the first study to provide a theoretical constraint on an upper bound of carbon export fluxes as a function of light availability, mixed layer depth and temperature.

References

Cael, B. B., and M. J. Follows (2016), On the temperature dependence of oceanic export efficiency, *Geophys Res Lett*, 43(10), 5170-5175.

Cael B. B., K. Bisson, and M. J. Follows (2017), How have recent temperature changes affected the efficiency of ocean biological carbon export? *Limnology and Oceanography Letters*, DOI: 10.1002/lol2.10042

Cassar, N., P. J. DiFiore, B. A. Barnett, M. L. Bender, A. R. Bowie, B. Tilbrook, K. Petrou, K. J. Westwood, S. W. Wright, and D. Lefevre (2011), The influence of iron and light on net community production in the Subantarctic and Polar Frontal Zones, *Biogeosciences*, 8(2), 227-237.

Dutkiewicz, S., M. Follows, J. Marshall, and W. W. Gregg (2001), Interannual variability of phytoplankton abundances in the North Atlantic, *Deep-Sea Res Pt II*, 48(10), 2323-2344.

Eveleth, R., N. Cassar, R. M. Sherrell, H. Ducklow, M. Meredith, H. Venables, Y. Lin, and Z. Li (2017), Ice melt influence on summertime net community production along the Western Antarctic Peninsula, *Deep Sea Research Part II*, 137, 89-102.

Gong, X., J. Shi, H. W. Gao, and X. H. Yao (2015), Steady-state solutions for subsurface chlorophyll maximum in stratified water columns with a bell-shaped vertical profile of chlorophyll, *Biogeosciences*, 12, 905-919.

Gong, X., W. Jiang, L. Wang, H. Gao, E. Boss, X. Yao, S. Kao, and J. Shi (2017), Analytical solution of the nitracline with the evolution of subsurface chlorophyll maximum in stratified water columns, *Biogeosciences*, 14, 2371-2386.

Huisman, J., N. N. P. Thi, D. M. Karl, and B. Sommeijer (2006), Reduced mixing generates oscillations and chaos in the oceanic deep chlorophyll maximum, *Nature*, 439, 322-325.

Taylor, J. R., R. Ferrari (2011), Shutdown of turbulent convection as a new criterion for the onset of spring phytoplankton blooms, *Limnol. Oceanogr.*, 56(6), 2293-2307.

Tortell, P. D., H. C. Bittig, A. Kortzinger, E. M. Jones, and M. Hoppema (2015), Biological and physical controls on N_2 , O_2 , and CO_2 distributions in contrasting Southern Ocean surface waters, *Global Biogeochem Cy*, 29(7), 994-1013.

Reviewer 2:

We thank the reviewer for his/her careful review of our manuscript. Below, we provide a response to the reviewer's comments which we think have significantly improved the quality of our manuscript:

Reviewer's comment: "This is a nice, clearly written paper, based on an interesting idea and executed well. The paper could be improved by clarifying the significance of the study somewhat. It may be very difficult ever to test or 'validate' this model properly. Yet, it is conceptually useful in some ways, e.g. the discussion about f_{pt} and nutrient limitation. The authors might want to discuss further, or clarify the existing discussion of, what the reader is supposed to have learned about the ocean."

Following the reviewer's comment, we now describe at the end of the introduction some of the key outcomes of our study:

"In our study, we build upon Sverdrup (1953) and derive a mechanistic model of an upper bound on carbon export based on the metabolic balance of photosynthesis and respiration in the oceanic mixed layer, where the metabolic balance is derived from MLD, temperature, photosynthetically active radiation (PAR), phytoplankton maximum growth rate (μ_{max}), and heterotrophic activity. Our approach is analogous to other efforts where mechanistic models were derived to predict proxies of carbon export (e.g., Dunne et al. (2005) and Cael and Follows (2016)). We compare our NCP^* model to observations, and use this model in conjunction with satellite export production estimates to identify regions in the world's oceans where light may limit export production. Our key findings are that 1) using parameters available in the literature, the modeled upper bound envelopes field observations of export production estimated from ^{234}Th and sediment traps and O_2/Ar -derived net community production, and 2) the model identifies regions of the Southern Ocean where carbon export is likely limited by light during part of the growing season."

Reviewer's comment: "There are several circumstances where the manuscript could be connected better to the literature. For instance, in line 30, there should be at least one

reference for this sentence (good references should be easy to find from the reference list in Boyd (2015) - same for the next sentence. Dunne et al (2005) and Cael and Follows (2016) develop mechanistic models to which this paper is very directly related, yet these models are mentioned only in passing.”

Following the reviewer’s recommendation, we now more explicitly make reference to the literature, including citations found in Boyd (2015). We agree with the reviewer that our effort is in the same vein as Dunne et al. (2005) and Cael and Follows (2016) and we now further emphasize the parallels in our approaches. The following references were added to the end of the first paragraph: “(Falkowski et al., 1998; Ito and Follows, 2005; Sigman and Boyle, 2000).” We also included references to Dunne et al. (2005) and Cael and Follows (2016) in the last paragraph of the introduction: “Our approach is analogous to other efforts where mechanistic models were derived to predict proxies of carbon export (e.g., Dunne et al. (2005) and Cael and Follows (2016)).”

Reviewer’s comment: “It is worth mentioning that not everyone loves the Sverdrup model (Behrenfeld, 2010), though using it in this context is a nice idea.”

We now refer to the competing models of “dilution recoupling hypothesis” or “disturbance recovery hypothesis” and “critical turbulence hypothesis” in the section on “caveats and limitations” and cite the relevant literature:

“In our study, we used a model which builds on Sverdrup’s critical depth hypothesis. There are competing hypotheses to explain phytoplankton bloom phenology (timing and intensity), including the “dilution recoupling hypothesis” or “disturbance recovery hypothesis” (Behrenfeld, 2010; Boss and Behrenfeld, 2010) and “critical turbulence hypothesis” (Brody and Lozier, 2015; Huisman et al., 1999; Taylor and Ferrari, 2011). In the case of top-down control, any respiratory grazing loss not accounted for by our loss term would behave as a system not reaching its full light potential (NCP*). Conversely, any grazing loss associated with export (e.g., rapidly sinking fecal pellets and other zooplankton-mediated export pathways) would minimize respiratory losses thereby bringing NCP closer to its upper bound based on light-availability. These opposing effects are beyond the scope of this study, but could be modeled, especially as we learn more about their impacts on carbon fluxes through new efforts such as NASA’s EXPORTS program (Siegel et al., 2016). See also the point below on mixing vs. mixed layer depth.”

Reviewer’s comment: “Some readers might also take issue with the sentence starting on line 31 - it’s better to say ‘export production is frequently assumed to be a function of’ (e.g. Estapa et al, 2015), though the rest of the paragraph deals with this nicely.”

We have modified the sentence following the reviewer’s comment to: “export production is frequently assumed to be a function of”.

Reviewer's comment: "It seems a bit ironic to compare this model, which is mechanistic, quite sophisticated, and carefully developed, with export data extrapolated using the Martin curve (an empirical parameterization) with a constant b-value. Granted, the model must be validated in some way, but the 'comparison to observations' subsection of the paper definitely appears to be its weak point."

A study recently published shows that the fit of the Martin curve to observations is as good as more sophisticated parameterizations which account for the ballast effect (Gloege et al. 2017). However, we agree with the reviewer that using the Martin curve to extrapolate the carbon export observations to the base of the mixed layer introduces uncertainties. To circumvent this issue, we now also present a figure in the supplementary material which only includes biological carbon fluxes directly measured within the mixed layer:

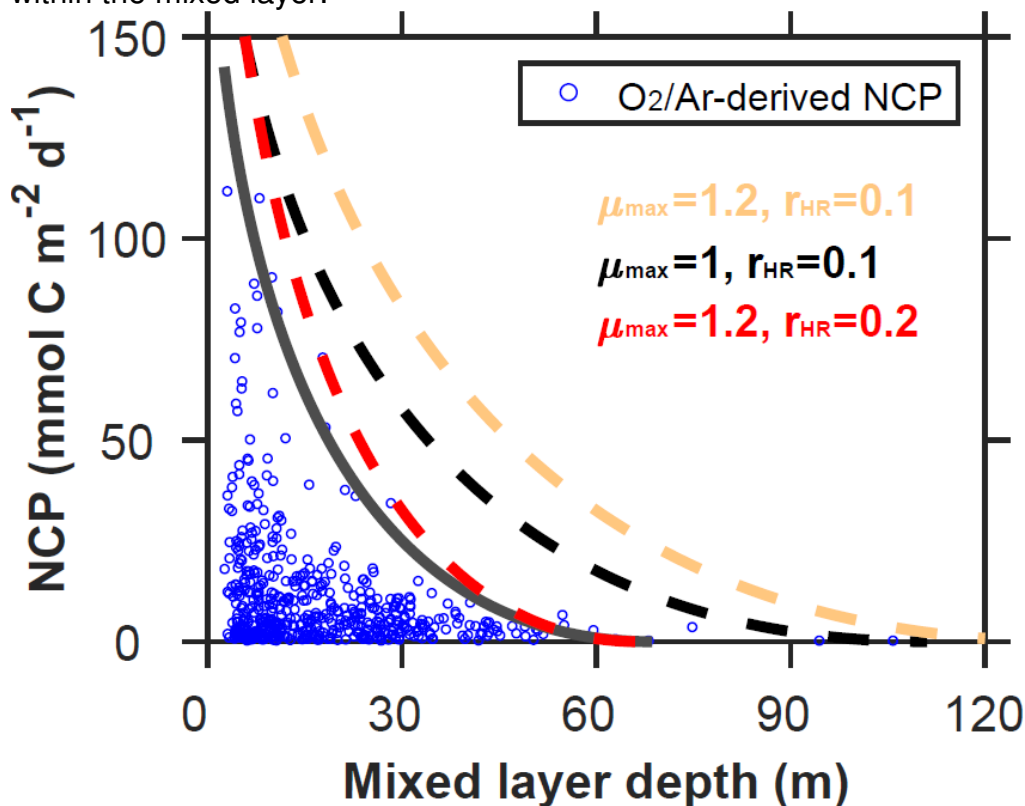


Figure S4. Modeled upper bound on carbon export production compared to field observations as a function of mixed layer depth (MLD). Observations are based on O₂/Ar-derived net community production (NCP). To account for the effect of photosynthetically active radiation (PAR) on export production, both MLD and carbon fluxes are normalized to $-\log(1 - I_m(0))$ (see equations (19) and (21)). The thick gray line represents the upper bound fitted to the NCP data. Dash-lines represent the upper bounds calculated using parameters available in the literature (Table 2). A stoichiometric ratio of O₂/C=1.4 was used to convert NCP from O₂ to C units (Laws, 1991).

Gloege, L., McKinley, G. A., Mouw, C. B., and Ciochetto, A. B.: Global evaluation of particulate organic carbon flux parameterizations and implications for atmospheric pCO₂, *Global Biogeochemical Cycles*, 2017.

Reviewer's comment: "Figures 3+4 are somewhat difficult to see/understand. The maps could be larger, and the axis limits could be chosen in a way to present the information more clearly."

Following the reviewer's comment, we have enlarged the maps, increased the resolution quality, and modified the axes scales.

The updated Figure 3 (Figure 4 in the revised manuscript) is shown below:

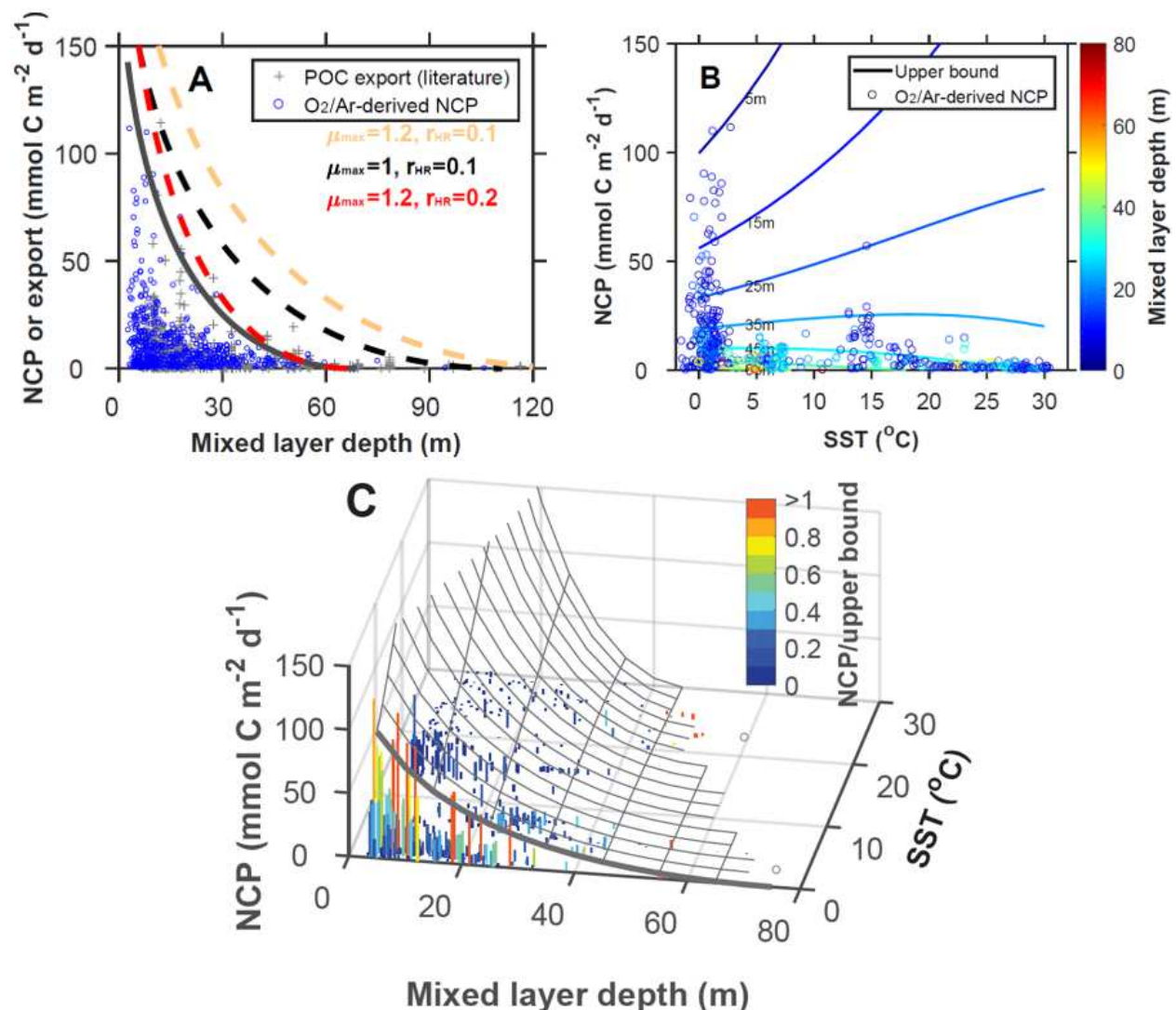


Figure 4. Modeled upper bound on carbon export production compared to field observations as a function of mixed layer depth (MLD) and sea surface temperature (SST). (A) The thick gray line represents the upper bound fitted to the net community production (NCP) data. Dash-lines represent the upper bounds calculated using

parameters available in the literature (Table 2). (B) NCP as a function of SST with isopleths of constant upper bounds color coded for MLD. NCP observations are color coded with MLD. (C) Surface representing the envelope of the modeled upper bound of carbon export production as a function of SST and MLD. Bars represent field observations color coded with the ratio of NCP to the upper bound. Observations are based on ^{234}Th and sediment traps estimates of carbon export production and O_2/Ar -derived NCP. A stoichiometric ratio of $\text{O}_2/\text{C}=1.4$ was used to convert NCP from O_2 to C units (Laws, 1991). To account for the effect of PAR on export production, both MLD and carbon fluxes are normalized to $-\log(1 - I_m(0))$ (see equations (19) and (21)). The temperature dependence of r_{HR} was modeled as $r_{HR} = r_{HR}^0 \times e^{0.08 \times T}$.

Reviewer's comment: "Eq. 21 may be missing a normalizing constant - a proportionality (Eq. 20) is not the same as an equals sign. The values of P_t and B_t both merit a bit more discussion -both numbers have some associated uncertainty, do they not?"

Following the reviewer's comment, we modified equations (20a) and (20b):

$$\mu_{max} = \mu_{max}^0 \times e^{P_t \times T} \quad (20a)$$

$$r_{HR} = r_{HR}^0 \times e^{B_t \times T} \quad (20b)$$

We also now elaborate on the uncertainties associated with both parameters. We modified the following paragraph in the section on caveats and limitations:

- μ_{max} and r_{HR} are influenced by environmental factors other than temperature, including community structure (Chen and Laws, 2017), and may vary with depth within the mixed layer. For these reasons, the equations relating μ_{max} and r_{HR} (i.e., B_t and P_t) to temperature carry uncertainties (Bissinger et al., 2008; Edwards et al., 2016; Kremer et al., 2017; López-Urrutia and Morán, 2007; Rivkin and Legendre, 2001) which impacts our estimates of the upper bound on carbon export, especially in warmer regions. As in other recent studies (Cael and Follows, 2016; Cael et al., 2017; Dutkiewicz et al., 2001; Gong et al., 2015; Gong et al., 2017; Huisman et al., 2006; Taylor and Ferrari, 2011), we model heterotrophic respiration to vary in proportion to phytoplankton concentration. The model could be further improved by explicitly including the concentration of heterotrophs. See point above on the grazing effect on export with regards to r_{HR} .

Reviewer 3:

We thank the reviewer for his/her insightful review of our manuscript. Below, we provide a response to the reviewer's comments which we think have significantly improved our manuscript.

Reviewer's comment: "The paper would benefit from more motivation for the model at the start. The introduction is fairly short and general. The reader would be more eager to dive into all the details of the model if the need for this model and the questions that the authors hope to address with it were clearly laid out near the beginning of the paper."

Figure 3 demonstrates that there are patterns in the observations that we should seek to explain, but this is only briefly introduced at the start of the paper. Figure 4 shows intuitive results, so here too the motivation to do the global analysis should be specifically stated.”

Following the reviewer’s comment, we now discuss the relevance of the study at the end of the third paragraph in the introduction:

Likewise, the effects of light and nutrient on carbon fluxes are difficult to disentangle. For example, high-nutrient, low-chlorophyll regimes in the Southern Ocean have been attributed to iron limitation (Boyd et al., 2000), deep mixed layers and light limitation (Nelson and Smith, 1991; Mitchell and Holm-Hanse, 1991; Mitchell et al., 1991), or both (Sunda and Huntsman, 1997). To decompose the influence of light and nutrient availability on NCP, we define the upper bound on carbon export from the mixed layer (NCP^*) as the maximum export achievable should all limiting factors other than light (taking into account self-shading) be alleviated.

Reviewer’s comment: “A large proportion of export is potentially controlled by bloom dynamics as phytoplankton escape heterotrophic grazing control or not. The proposed model misses these dynamics by forcing heterotrophic respiration to be solely proportional to phytoplankton concentration, rather than also include heterotroph concentrations. Of course, this simplifies the model considerably. However, this simplification may render the results irrelevant since the model then does not approximate the real system closely enough. At the very least, the authors need to carefully argue that their model remains valid for the questions they wish to address despite this simplification of heterotrophic respiration. Such an argument is presently missing from the paper.”

We now better acknowledge this limitation in our revised manuscript, including in the section on caveats and limitations where we expand on grazing and heterotrophy. We now also cite additional papers where a similar approach has been used (e.g., Cael and Follows, 2016, Cael et al., 2017, Dutkiewicz et al., 2001, Gong et al., 2015, Gong et al., 2017, Huisman et al., 2006, and Taylor and Ferrari, 2011).

In the section on caveats and limitations, we added the following paragraph:

- μ_{max} and r_{HR} are influenced by environmental factors other than temperature, including community structure (Chen and Laws, 2017), and may vary with depth within the mixed layer. For these reasons, the equations relating μ_{max} and r_{HR} (i.e., B_t and P_t) to temperature carry uncertainties (Bissinger et al., 2008; Edwards et al., 2016; Kremer et al., 2017; López-Urrutia and Morán, 2007; Rivkin and Legendre, 2001) which impacts our estimates of the upper bound on carbon export, especially in warmer regions. As in other recent studies (Cael and Follows, 2016; Cael et al., 2017; Dutkiewicz et al., 2001; Gong et al., 2015; Gong et al., 2017; Huisman et al., 2006; Taylor and Ferrari, 2011), we model heterotrophic respiration to vary in proportion to phytoplankton concentration. The model could be further

improved by explicitly including the concentration of heterotrophs. See point above on the grazing effect on export with regards to r_{HR} .

Reviewer's comment: "I would like to see more clarity about how the generalized conclusions of the model depend on choices for specific constants. For example, the discussion in the paragraph beginning on line 121 only holds where k_c is significant. As k_c goes toward zero, selfshading decreases and NPP will continuously increase as C increases. The text is not clear on whether the k_c required to cause the self-shading induced decrease in $dNCP/dC$ above a certain C is reasonable. The paper discusses specific values for some of these constants later in section 2.5, but it seems as though the values of these constants affect earlier conclusions as well."

Because pure water and phytoplankton attenuate light, K_l^w and k_c must be greater than zero. Over the range of k_c values reported in the literature, the behavior of $dNCP/dC$ is not expected to change, as now clarified in the manuscript. Following the reviewer's comment, we now also include a new table (Table 2) which shows the value or range of values (and references) associated with the constants used.

Reviewer's comment: "The simplification in the last part of equation 15 appears to remove the dependence of average mixed layer irradiance on the depth of the mixed layer. Equation 16, based on this simplification, demonstrates that only the respiration term is now sensitive to the mixed layer depth (MLD cancels from the first term). This seems to run counter to all the previous arguments that MLD is important to integrated NPP values."

This is an important point raised by the reviewer. We have now revised the approximation in Equation (15). Below, we show a figure showing the comparison of upper bounds derived using the original and approximated models. As can be seen, the difference in behavior is small. However, we now include this figure in the manuscript.

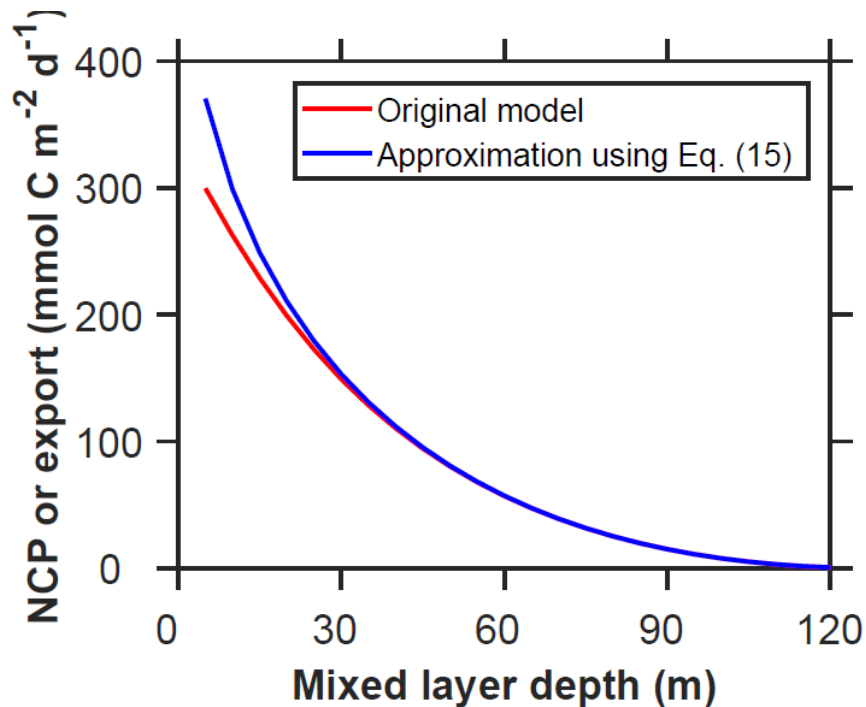


Figure 3. Upper bounds derived using the original and approximated models. The upper bound for the original model (equations (8-10)) is estimated through a non-linear optimization approach. The upper bound for the approximated model is calculated analytically from equation (19). The models use the constants listed in Table 2 and $I_m(0) = 0.9$. Decreasing $I_m(0)$ and increasing r_{HR} results in greater discrepancies between the original and approximated models in regions with shallow mixed layers.

Reviewer's comment: "Lines 51-56: The discussion of attribution of these patterns seems too limited. Low NCP at high temperatures could be primarily a function of a tendency toward increased stratification and nutrient limitation in warm waters. Additionally, deep mixed layers can bias the O₂/Ar method low if entrainment of deeper waters brings low oxygen into the mixed layer."

In the section on caveats and limitations, we mention that the field observations harbor significant uncertainties. In the same bullet point, we now mention as an example that "deep mixed layers can bias the O₂/Ar method low if entrainment of deeper waters brings low O₂ into the mixed layer".

On line 275 of the original manuscript, we now further elaborate on the low f_{pt} in warm waters. These waters cannot reach their full export potential because of increased stratification and nutrient limitation ("The ultra-oligotrophic subtropical waters have a low export ratio, a strong biological pump efficiency with exhaustion of nutrients at the ocean surface, and therefore have not reached their full light potential (low f_{pt}) because of the strong stratification and nutrient limitation").

Reviewer's comment: "Line 82: "light" attenuation coefficient rather than "diffusion" attenuation coefficient?"

The term "light" attenuation coefficient has been replaced with "diffusion" attenuation coefficient.

Reviewer's comment: "Lines 113-120 and following paragraph: This section is unclear in places. Figure 2 could be actively discussed to demonstrate why $dNCP/dC$ asymptotes at $-r^*MLD$ through comparison of the production and respiration terms on the right side of Figure 2a where the production term becomes stable. I spent a long time thinking about this, so the authors could really lead the reader through these arguments better. The text implies in places that $dNCP/dC$ always decreases with increasing C (lines 113-114), but this is only the case at C larger than C^* ."

As stated in our original manuscript, $dNCP/dC$ systematically decreases with increasing C (this is because $\frac{d^2NCP(0,MLD)}{dC^2}$ is smaller than zero (see equation 12)). However, $dNCP/dC$ remains positive below C^* , and becomes negative above C^* . Following the reviewer's comment, we now discuss the asymptote of $\frac{dNCP(0,MLD)}{dC}$ using Figure 2: "Because increasing C decreases light availability due to self-shading, $NPP(0,MLD)$ saturates with increasing C . Thus, $NCP(0,MLD)$ will reach an asymptote of $\lim_{C \rightarrow \infty} \left(\frac{dNCP(0,MLD)}{dC} \right) = -r_{HR} \times MLD < 0$, because $HR(0,MLD)$ linearly increases with increasing C while $NPP(0,MLD)$ plateaus (Figure 2)."

Reviewer's comment: "Lines 138-140: the statement here that integrated NCP is maximized when the MLD is below the compensation depth seems contrary to the schematic representation of the system in Figure 1a vs. 1b where the integrated NCP is maximized at the compensation depth."

The compensation depth is a function of C . In Figure 1, C is assumed to be constant and MLD is allowed to vary (e.g., synoptic variability in MLD). In this case, depth-integrated NCP will be maximized when MLD deepens or shoals to the compensation depth. Conversely, in (equation 14), C is allowed to vary for a given MLD (e.g., stable water column with varying phytoplankton biomass), in which case, the compensation depth will respond and the depth-integrated NCP peaks when the mixed layer is slightly deeper than the compensation depth.

We amended the manuscript with the following sentence: "We note that in equation (14) the NCP profile ($NCP(z)$) varies with increasing C , which is different from what is conceptually presented in Figure 1. The depth-integrated NCP in Figure 1 maximizes at the compensation depth because the NCP profile ($NCP(z)$) is assumed to be invariant."

Reviewer’s comment: “Line 163: Why the MLD should satisfy the given conditions are not clear here until Line 171, where the authors state that they have chosen not to consider other possibilities.”

Following the reviewer’s comment, we reorganized the sentences:

“Equation (18) decreases with MLD. As C^* is positive ($C^* \geq 0$) and cannot go to infinity ($C^* \leq C_{max}^*$), MLD should satisfy $MLD_{C_{max}^*} \leq MLD \leq \frac{\mu^*}{r_{HR} \times K_I^w}$, where $MLD_{C_{max}^*}$ represents the MLD corresponding to the maximum achievable autotroph’s biomass concentration (C_{max}^*) in the surface ocean. The NCP^* model for $0 \leq MLD < MLD_{C_{max}^*}$ is not discussed here, because we do not have data with very shallow MLD to constrain and evaluate the model. The derivation of the model is however presented in the supplementary material.”

Reviewer’s comment: “Equations 20a and 20b: These are written as simple proportionalities here, but later treated as though the proportional sign is replaced with an equal sign. It seems like there should be an additional constant.”

Following the reviewer’s comment, we modified equations (20a) and (20b):

$$\mu_{max} = \mu_{max}^0 \times e^{P_t \times T} \quad (20a)$$

$$r_{HR} = r_{HR}^0 \times e^{B_t \times T} \quad (20b)$$

Reviewer’s comment: “Section 2.5: Where specific values or ranges of values are chosen for model constants, it would be helpful to list these in the table defining notation.”

Following the reviewer’s comment, we added a table that includes the typical range of the parameters with references.

Table 2. Value or range of values with references for the parameters used in the model

Parameter	Range or value	Reference
K_I^w	0.09	(Werdell and Bailey, 2005)
k_c	0.03	(Werdell and Bailey, 2005)
Carbon to chlorophyll ratio	90	(Arrigo et al., 2008)
k_m^I	4.1 Einstein $m^{-2} d^{-1}$	(Behrenfeld and Falkowski, 1997)
P_t	0.0663	(Eppley, 1972)
B_t	0.08	(Rivkin and Legendre, 2001; López-Urrutia et al., 2006)
μ_{max}	1 d^{-1} , 1.2 d^{-1}	(Laws et al., 2000; Eppley, 1972)
r_{HR}	0.1 d^{-1} , 0.2 d^{-1}	(Laws et al., 2000; Mitchell et al., 1991)

Reviewer's comment: "Line 196: It's unclear why data could be below the theoretical line due to light limitation, when the theoretical line is specifically modeled to include light limitation."

Following the reviewer's comment, we have removed the reference to light limitation in the sentence. Now: "Conversely, points below the upper bound may be nutrient limited."

Reviewer's comment: "Model-data differences are difficult to clearly discern in Figure 3b. Perhaps it would be useful to directly plot model-data differences in a third panel. That the NCP* model performs poorly in warm deep mixed layers (as stated on lines 210-211) cannot be clearly seen in the figure."

Following the reviewer's comment, we added a panel in the original Figure 3 (now Figure 4) showing the upper bound as a function of SST with isopleths of constant upper bounds color coded for MLD.

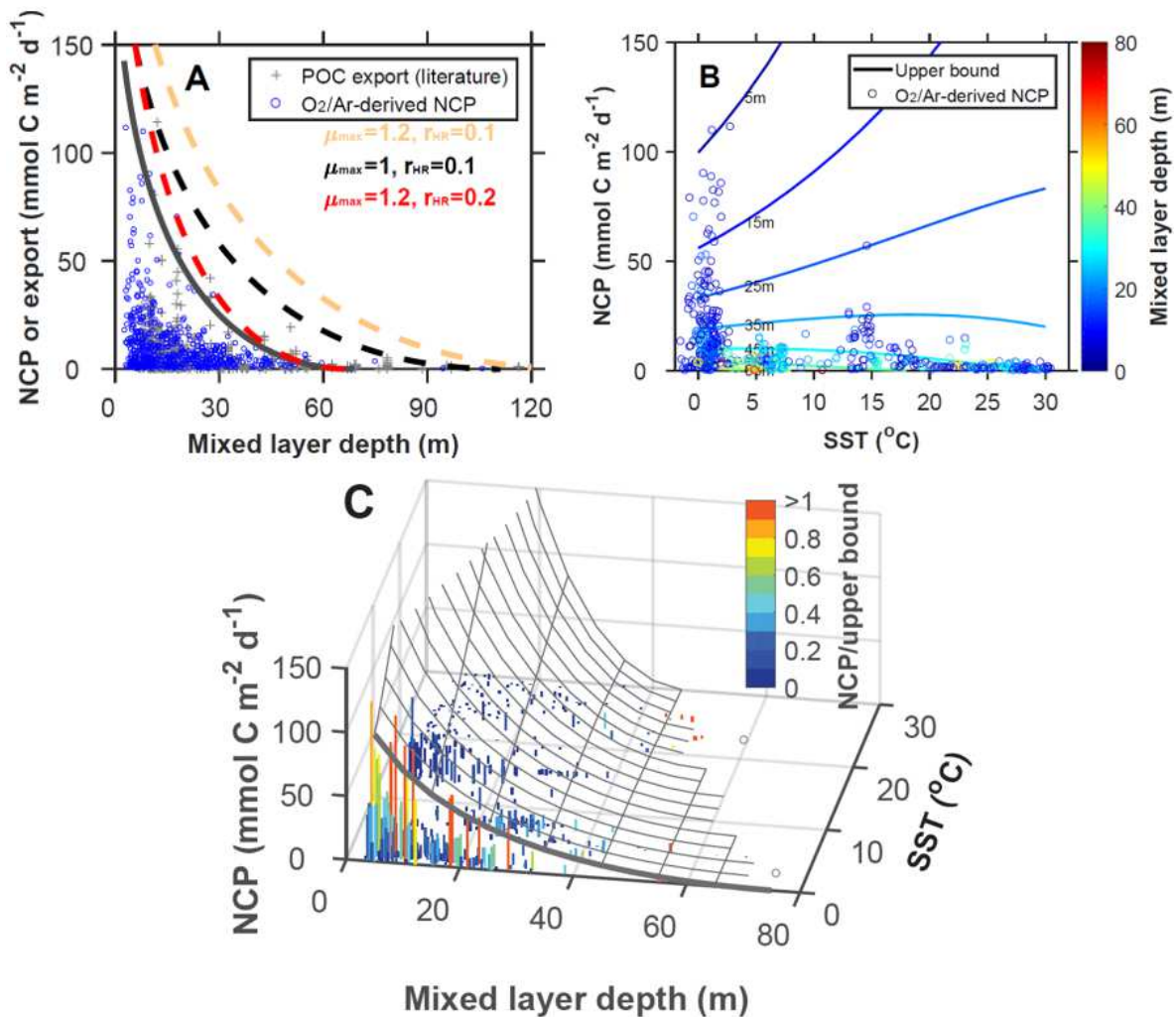


Figure 4. Modeled upper bound on carbon export production compared to field observations as a function of mixed layer depth (MLD) and sea surface temperature (SST). (A) The thick gray line represents the upper bound fitted to the net community production (NCP) data. Dash-lines represent the upper bounds calculated using parameters available in the literature (Table 2). (B) NCP as a function of SST with isopleths of constant upper bounds color coded for MLD. NCP observations are color coded with MLD. (C) Surface representing the envelope of the modeled upper bound of carbon export production as a function of SST and MLD. Bars represent field observations color coded with the ratio of NCP to the upper bound. Observations are based on ^{234}Th and sediment traps estimates of carbon export production and O_2/Ar -derived NCP. A stoichiometric ratio of $\text{O}_2/\text{C}=1.4$ was used to convert NCP from O_2 to C units (Laws, 1991). To account for the effect of PAR on export production, both MLD and carbon fluxes are normalized to $-\log(1 - I_m(0))$ (see equations (19) and (21)). The temperature dependence of r_{HR} was modeled as $r_{HR} = r_{HR}^0 \times e^{0.08 \times T}$.

Reviewer's comment: "Line 281: The text discusses discrepancies between predicted and observed NCP*. However, only NCP can be observed, not NCP*."

We agree with the reviewer. The sentence has been modified to: "There are a multitude of uncertainties, simplifications, and approximations in our model and field observations. Among others:"

1 **A mechanistic model of an upper bound on oceanic carbon export as a**
2 **function of mixed layer depth and temperature**

3 Zuchuan Li*, Nicolas Cassar

4 Division of Earth and Ocean Sciences, Nicholas School of the Environment, Duke University,
5 Durham, North Carolina, USA

6
7 * Corresponding author: Zuchuan Li (zuchuan.li@duke.edu)

8
9
10 **Key points**

11 1. A mechanistic model of an upper bound on carbon export is developed based on the metabolic
12 balance of photosynthesis and respiration in the oceanic mixed layer

13 2. Using parameters available in the literature, the modeled upper bound envelopes field
14 observations of export production estimated from ²³⁴Th and sediment traps and O₂/Ar-derived net
15 community production

16 3. The model identifies regions of the Southern Ocean where carbon export is likely limited by
17 light during part of the growing season

21 **Abstract**

22 Export production reflects the amount of organic matter transferred from the surface ocean to depth
23 through biological processes. This export is in great part controlled by nutrient and light
24 availability, which are conditioned by mixed layer depth (MLD). In this study, building on
25 Sverdrup's critical depth hypothesis, we derive a mechanistic model of an upper bound on carbon
26 export based on the metabolic balance between photosynthesis and respiration as a function of
27 MLD and temperature. We find that the upper bound is a positively skewed bell-shaped function
28 of MLD. Specifically, the upper bound increases with deepening mixed layers down to a critical
29 depth, beyond which a long tail of decreasing carbon export is associated with increasing
30 heterotrophic activity and decreasing light availability. We also show that in cold regions the upper
31 bound on carbon export decreases with increasing temperature when mixed layers are deep, but
32 increases with temperature when mixed layers are shallow. A metaanalysis shows that our model
33 envelopes field estimates of carbon export from the mixed layer. When compared to satellite export
34 production estimates, our model indicates that export production in some regions of the Southern
35 Ocean, most particularly the Subantarctic Zone, is likely limited by light for a significant portion
36 of the growing season.

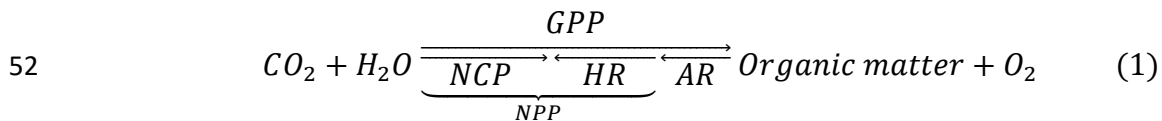
37 **Key words:** Export production, net community production, upper bound, mixed layer depth,
38 temperature

39

40 **1. Introduction**

41 Photosynthesis in excess of respiration at the ocean surface leads to the production of organic
42 matter, part of which is transported to the deep ocean through sinking and mixing (Volk and
43 Hoffert, 1985). This biological process, known as export production (aka soft tissue biological
44 carbon pump) lowers carbon dioxide (CO₂) concentrations at the ocean surface and facilitates the
45 flux of CO₂ from the atmosphere into the ocean ([Falkowski et al., 1998](#); [Ito and Follows, 2005](#);
46 [Sigman and Boyle, 2000](#)).

47 Export production is [frequently assumed to be](#) a function of net community production (NCP)
48 which is defined as the balance between net primary production (NPP) and heterotrophic
49 respiration (HR), or the difference between gross primary production (GPP) and community
50 respiration (CR; HR plus autotrophic respiration (AR)) (the acronyms used in this study are
51 presented in Table 1) ([Li and Cassar, 2016](#)):



53
$$Export\ production = NCP - MLD \times \frac{d(POC + DOC)}{dt} \quad (2)$$

54 where POC, DOC and MLD represent particulate organic carbon, dissolved organic carbon and
55 mixed layer depth, respectively. If the organic carbon inventory (POC+DOC) in the mixed layer
56 is at steady state, NCP is equal to export production (equation (2)). Without allochthonous sources
57 of organic matter, if the organic matter inventory in the mixed layer decreases, NCP will be
58 predicted to be transiently smaller than export production. Conversely, export may lag NPP
59 (Henson et al., 2015; Stange et al., 2017), in which case NCP is expected to be greater than export
60 production.

61 Net community production is in great part regulated by the availability of nutrients and light.
62 Light availability exponentially decays with depth due to absorption by water and its constituents.
63 The mixing of phytoplankton to depth therefore impacts phytoplankton physiology and
64 productivity (Cullen and Lewis, 1988; Lewis et al., 1984), with the depth-integrated NPP expected
65 to increase down to the euphotic depth. Respiration, on the other hand, is often modeled to be some
66 function of organic matter concentration, which is expected to be constant with depth if
67 homogeneously mixed within the mixed layer. Temperature is also believed to be an important
68 control on carbon export because respiration is more temperature-sensitive than photosynthesis
69 (Laws et al., 2000; López-Urrutia et al., 2006; Rivkin and Legendre, 2001). Field observations
70 confirm that NCP is generally lower at high temperatures and consistently low when mixed layers
71 are deep. These patterns have been attributed to the balance between depth-integrated
72 photosynthesis (controlled by the availability of nutrients and light) and respiration as a function
73 of MLD and temperature (Cassar et al., 2011; Eveleth et al., 2016; Huang et al., 2012; Shadwick
74 et al., 2015; Tortell et al., 2015). However, descriptions of the underlying mechanisms heretofore
75 remain qualitative. Likewise, the effects of light and nutrient on carbon fluxes are difficult to
76 disentangle. For example, high-nutrient, low-chlorophyll regimes in the Southern Ocean have been
77 attributed to iron limitation (Boyd et al., 2000), deep mixed layers and light limitation (Nelson and
78 Smith, 1991; Mitchell and Holm-Hanse, 1991; Mitchell et al., 1991), or both (Sunda and Huntsman,
79 1997). To decompose the influence of light and nutrient availability on NCP, we define the
80 upper bound on carbon export (NCP^*)—from the mixed layer (NCP^*) as the maximum export
81 achievable should all limiting factors other than light (e.g., nutrient taking into account self-
82 shading) be alleviated.

83 In his seminal paper, Sverdrup presented an elegant model to demonstrate that vernal
84 phytoplankton blooms (i.e., organic matter accumulation at the ocean surface) may be driven by
85 increased light availability when the MLD shoals above a critical depth (Z_c) (Sverdrup, 1953). In
86 our study, we build upon Sverdrup (1953) and derive a mechanistic model of an upper bound on
87 carbon export based on the metabolic balance of photosynthesis and respiration in the oceanic
88 mixed layer, where the metabolic balance is derived from ~~with respect to~~ MLD, temperature,
89 photosynthetically active radiation (PAR), phytoplankton maximum growth rate (μ_{max}), and
90 heterotrophic activity. Our approach is analogous to other efforts where mechanistic models were
91 derived to predict proxies of carbon export (e.g., Dunne et al. (2005) and Cael and Follows (2016)).
92 We compare our *NCP** model to observations, and use this model in conjunction with satellite
93 export production estimates to identify regions in the world's oceans where light may limit export
94 production. Our key findings are that 1) using parameters available in the literature, the modeled
95 upper bound envelopes field observations of export production estimated from ^{234}Th and sediment
96 traps and O_2/Ar -derived NCP, and 2) the model identifies regions of the Southern Ocean where
97 carbon export is likely limited by light during part of the growing season.

98 **2. Model description and comparison to observations**

99 **2.1. Net community production and light availability**

100 A conceptual representation of the metabolic balance between volumetric NCP, NPP, and HR
101 profiles is presented in Figure 1(A). According to equation (1), the volumetric NCP flux at a given
102 depth (z) in the mixed layer results from the difference between volumetric NPP and HR:

$$103 \quad NCP(z) = NPP(z) - HR(z) \quad (3)$$

104 where z increases with depth. $NPP(z)$ is a function of the autotroph's intrinsic growth rate
105 (μ) times their biomass concentration (C). Assuming that the effect of nutrients and light on

106 photosynthetic rates abides by Michaelis-Menten kinetics, and neglecting the effect of
 107 photoinhibition (Dutkiewicz et al., 2001; Huisman and Weissing, 1994), $NPP(z)$ may be
 108 expressed as follows:

$$109 \quad NPP(z) = \mu(z) \times C = \frac{N}{N + k_m^N} \times \frac{I(z)}{I(z) + k_m^I} \times \mu_{max} \times C \quad (4)$$

110 where μ_{max} is the maximum intrinsic growth rate of the autotrophic community; N and k_m^N
 111 represent the nutrient concentration and half-saturation constant, respectively; and I and k_m^I
 112 represent the irradiance level and half-saturation constant, respectively. μ_{max} , N , k_m^N , k_m^I and C
 113 are assumed to be well mixed within the mixed layer. The first two terms on the right-hand side of
 114 equation (4) account for the effect of nutrient and light availability on autotrophic growth rates,
 115 and they are hereafter defined as follows for simplicity:

$$116 \quad N_m = \frac{N}{N + k_m^N} \quad (5a)$$

$$117 \quad I_m(z) = \frac{I(z)}{I(z) + k_m^I} \quad (5b)$$

118 $I(z)$ is modeled as an exponential decay of PAR just beneath the water surface (I_0):

$$119 \quad I(z) = I_0 \times e^{-K_I \times z} \quad (6)$$

120 where K_I is ~~diffusion-light~~ attenuation coefficient which is assumed to be independent of depth in
 121 the mixed layer.

122 As a first approximation, we assume that $HR(z)$ is proportional to C as in previous studies
 123 (Dutkiewicz et al., 2001; Huisman and Weissing, 1994; Rivkin and Legendre, 2001; Sverdrup,
 124 1953; White et al., 1991):

$$125 \quad HR(z) = r_{HR} \times C \quad (7)$$

126 where r_{HR} represents the intrinsic heterotrophic respiration rate which is assumed to be dependent
 127 on temperature (see below), and independent of depth. In reality, $HR(z)$ is likely best modeled as
 128 a function of the concentration of labile organic matter — an additional term could be included to
 129 account for the relationship of total labile organic matter to C .

130 NCP integrated over the mixed layer ($NCP(0, MLD)$) can be derived from equations (3-7):

$$\begin{aligned}
 131 \quad NCP(0, MLD) &= NPP(0, MLD) - HR(0, MLD) \\
 132 \quad &= \int_0^{MLD} NPP(z) dz - \int_0^{MLD} HR(z) dz \\
 133 \quad &= N_m \times I_m(0, MLD) \times \mu_{max} \times C - r_{HR} \times MLD \times C \quad (8)
 \end{aligned}$$

134 The first term on the right side of equation (8) represents NPP integrated over the mixed layer
 135 ($NPP(0, MLD)$), which is equivalent to the product of $\int_0^{MLD} \mu(z) dz$ and C , where the former term
 136 is modeled to be a function of μ_{max} conditioned by nutrient and light availability within the mixed
 137 layer. $I_m(0, MLD)$ can be derived as follows:

$$138 \quad I_m(0, MLD) = \int_0^{MLD} I_m(z) dz = -\frac{1}{K_I} \times \ln \left(\frac{I_0 \times e^{-K_I \times MLD} + k_m^I}{I_0 + k_m^I} \right) \quad (9)$$

139 NCP integrated over the mixed layer (equation (8)) is a bell-shaped function of MLD as depicted
 140 in the schematic diagram of Figure 1(B).

141 **2.2. Net community production and phytoplankton biomass concentration**

142 As can be seen from equation (8), $NCP(0, MLD)$ is a direct function of C because
 143 $NPP(0, MLD)$ and $HR(0, MLD)$ are proportional to C . $NCP(0, MLD)$ is also an indirect function
 144 of C due its effect on light attenuation (i.e., K_I). The attenuation coefficient K_I can be divided into
 145 water and non-water components ($K_I = K_I^w + K_I^{nw}$) (Baker and Smith, 1982; Smith and Baker,
 146 1978a; Smith and Baker, 1978b), where K_I^{nw} is controlled by the concentrations of phytoplankton,
 147 colored dissolved organic matter (CDOM), and non-algal particles (NAP). In the open ocean where

148 CDOM and NAP co-vary with phytoplankton (Morel and Prieur, 1977), K_I can be related to C as
 149 follows:

$$150 \quad K_I = K_I^w + k_c \times C \quad (10)$$

151 where k_c is a function of the solar zenith angle, the specific absorption and backscattering
 152 coefficients of phytoplankton, and the relationship between phytoplankton, CDOM, and NAP.

153 Because pure water and phytoplankton attenuate light, K_I^w and k_c should be greater than zero.

154 To calculate how $NCP(0, MLD)$ varies as a function of C , we examine its first ($\frac{dNCP(0,MLD)}{dC}$)
 155 and second ($\frac{d^2NCP(0,MLD)}{dC^2}$) derivatives with respect to C based on equations (8) and (10):

$$156 \quad \frac{dNCP(0, MLD)}{dC}$$

$$157 \quad = N_m \times \mu_{max} \times \frac{K_I^w \times I_m(0, MLD) + k_c \times C \times MLD \times I_m(MLD)}{K_I^w + k_c \times C} - r_{HR} \times MLD \quad (11)$$

$$158 \quad \frac{d^2NCP(0, MLD)}{dC^2} = N_m \times k_c \times \frac{\mu_{max}}{K_I}$$

$$159 \quad \times \left\{ \frac{2 \times K_I^w}{K_I} \times (MLD \times I_m(MLD) - I_m(0, MLD)) - \frac{k_c \times C \times I_m(MLD)^2 \times MLD^2 \times k_m^l}{I_0 \times e^{-K_I \times MLD}} \right\} \quad (12)$$

160 when $MLD > 0$, $I_m(0, MLD) > MLD \times I_m(MLD)$:

$$161 \quad I_m(0, MLD) = \int_0^{MLD} \frac{I_0 \times e^{-K_I \times z}}{I_0 \times e^{-K_I \times z} + k_m^l} dz$$

$$162 \quad > \int_0^{MLD} \frac{I_0 \times e^{-K_I \times MLD}}{I_0 \times e^{-K_I \times MLD} + k_m^l} dz = MLD \times I_m(MLD) \quad (13)$$

163 The detailed derivation of equations (11-12) can be found in the supplementary material.

164 Substituting the inequality (13) into equation (12) gives $\frac{d^2NCP(0,MLD)}{dC^2} < 0$, which suggests that

165 $\frac{dNCP(0,MLD)}{dC}$ decreases with increasing C . Because increasing C decreases light availability due to

166 shelf-shading, $NPP(0, MLD)$ saturate with increasing C . Thus, $NCP(0, MLD)$ will reach an
 167 asymptote of $\lim_{C \rightarrow \infty} \left(\frac{dNCP(0, MLD)}{dC} \right) = -r_{HR} \times MLD < 0$, because $HR(0, MLD)$ linearly increases
 168 with increasing C while $NPP(0, MLD)$ plateaus (Figure 2). ~~reaching an asymptote of~~
 169 ~~$\lim_{C \rightarrow \infty} \left(\frac{dNCP(0, MLD)}{dC} \right) = -r_{HR} \times MLD < 0$ (Figure 2(B)).~~ Additionally, because $NCP(0, MLD)$ must
 170 be nil when there is no autotrophic biomass ($NCP(0, MLD)|_{C=0} = 0$), $\lim_{C \rightarrow 0} \left(\frac{dNCP(0, MLD)}{dC} \right)$ must be
 171 ~~larger~~ greater than zero θ , otherwise the ecosystem would be net heterotrophic which is
 172 unachievable without an allochthonous source of organic matter. $\lim_{C \rightarrow 0} \left(\frac{dNCP(0, MLD)}{dC} \right) > 0$ and
 173 $\lim_{C \rightarrow \infty} \left(\frac{dNCP(0, MLD)}{dC} \right) = -r_{HR} \times MLD < 0$ suggest the existence of $\left. \frac{dNCP(0, MLD)}{dC} \right|_{C=C^*} = 0$ where C^*
 174 corresponds to an autotrophic biomass concentration which maximizes $NCP(0, MLD)$ (i.e., NCP^*).

175 The dependence of $NCP(0, MLD)$ on C can be conceptually understood in the following way.
 176 Given a water column with sufficient nutrients, the critical depth Z_c and compensation depth Z_p
 177 are expected to shoal as C increases. When C is low, $NCP(0, MLD)$ increases with C because of
 178 its greater impact on $NPP(0, MLD)$ than on $HR(0, MLD)$. As C further increases, the increase in
 179 $NPP(0, MLD)$ with C slows because of light attenuation (i.e., K_l). There is therefore a C^* which
 180 maximizes the difference between $NPP(0, MLD)$ and $HR(0, MLD)$ leading to NCP^* (Figure 2).
 181 Beyond this point (C^*), further increasing C will cause self-shading and limit photosynthesis in the
 182 deep part of the mixed layer, as a result decreasing $NCP(0, MLD)$. Beyond a critical biomass (C_c),
 183 the ecosystem becomes net heterotrophic. Without an allochthonous source of organic carbon, this
 184 is only transiently sustainable.

185 2.3. Mixed layer depth and compensation depth

186 By definition, if $NCP(MLD)$ is smaller than zero (i.e., net heterotrophy at the bottom of the
 187 mixed layer), the MLD must be deeper than Z_p ($MLD > Z_p$) (and vice versa). To determine the

188 sign of $NCP(MLD)$, we substitute inequality (13) into equation (11). According to the inequality
 189 presented in equation (13), $\frac{K_l^w \times I_m(0,MLD) + k_c \times C \times MLD \times I_m(MLD)}{K_l^w + k_c \times C}$ in equation (11) must be larger-greater
 190 than $\frac{K_l^w \times MLD \times I_m(MLD) + k_c \times C \times MLD \times I_m(MLD)}{K_l^w + k_c \times C}$ (which is equal to $MLD \times I_m(MLD)$). After simple
 191 rearrangements, the substitution of inequality (13) into equation (11) leads to:

$$\begin{aligned}
 & \frac{dNCP(0, MLD)}{dC} \\
 & > MLD \times (N_m \times I_m(MLD) \times \mu_{max} - r_{HR}) = \frac{MLD}{C} \times NCP(MLD) \quad (14)
 \end{aligned}$$

194 The inequality in equation (14) in turn suggests that when $NCP(0,MLD)$ is maximized
 195 ($\frac{dNCP(0,MLD)}{dC} = 0$), $NCP(MLD)$ is negative (net heterotrophic) and hence the MLD is deeper than
 196 Z_p ($MLD > Z_p$). This counterintuitive result is attributable both to the uneven distribution of light
 197 availability in the water column (equation (13)) and to water which absorbs light but does not
 198 contribute to biomass accumulation. When the mixed layer is at the Z_p , a slight increase in C will
 199 leads to negative $NCP(MLD)$ due to decreasing light availability at the base of mixed layer, but
 200 will increase NCP higher in the water column because of the increase in biomass. The increase in
 201 NCP in the shallow parts of the mixed layer therefore overcompensates for the net heterotrophy at
 202 the bottom of the mixed layer, thus maximizing the depth-integrated NCP. If light were uniformly
 203 distributed in the water column (i.e., $I_m(0,MLD) = MLD \times I_m(MLD)$) and if water did not
 204 attenuate light ($K_l^w = 0$ in equation (11)), $MLD = Z_p$ would maximize $NCP(0,MLD)$, which is
 205 consistent with Huisman and Weissing (1994). We note that in equation (14) the NCP profile
 206 ($NCP(z)$) varies with increasing C , which is different from what is conceptually presented in
 207 Figure 1. The depth-integrated NCP in Figure 1 maximizes at the compensation depth because the
 208 NCP profile ($NCP(z)$) is assumed to be invariant.

209 **2.4. An upper bound on carbon export**

210 Equations (11-13) delineate the conditions for an upper bound on carbon export (NCP^*). In
 211 order to simplify the relationship of NCP^* to MLD and temperature, we approximate $I_m(0, MLD)$:

$$\begin{aligned}
 212 \quad I_m(0, MLD) &= -\frac{1}{K_I} \times \ln \left(1 + \frac{I_0}{I_0 + k_m^I} \times (e^{-K_I \times MLD} - 1) \right) \\
 213 \quad &\approx \frac{I_m(0) \times \frac{1 - e^{-K_I \times MLD}}{K_I}}{K_I} - \frac{1}{K_I} \times \ln(1 - I_m(0)) \\
 214 \quad &\approx \frac{I_m(0) \times \frac{1}{K_I}}{K_I} \quad (15)
 \end{aligned}$$

215 where $I_m(0) = \frac{I_0}{I_0 + k_m^I}$. Based on equation (15), $NCP(0, MLD)$ in equation (8) can be approximated
 216 as:

$$217 \quad NCP(0, MLD) = C \times MLD \times \left(\frac{1}{K_I \times MLD} \times \mu^* - r_{HR} \right) \quad (16)$$

218 where $\mu^* = \frac{I_m(0)}{K_I} - \ln(1 - I_m(0)) \times N_m \times \mu_{max}$. To evaluate the approximation accuracy of
 219 equation (15), we compare the upper bounds estimated from equation (16) and the original model
 220 (equations (8-10)). Our comparison suggests that the approximation of equation (15) is accurate
 221 for the estimation of NCP^* under most conditions (Figure 3).

222 We first need to derive the C^* which maximizes $NCP(0, MLD)$ (i.e., NCP^*) in equation (16).
 223 C^* can be solved from the first derivative of $NCP(0, MLD)$ in equation (16) with respect to C :

$$224 \quad \left. \frac{dNCP(0, MLD)}{dC} \right|_{NCP(0, MLD)=NCP^*} = \mu^* \times \frac{K_I^W}{(k_c \times C^* + K_I^W)^2} - MLD \times r_{HR} = 0 \quad (17)$$

225
 226 and therefore:

$$227 \quad C^* = \frac{1}{k_c} \times \left[-K_I^W + \sqrt{\frac{\mu^* \times K_I^W}{MLD \times r_{HR}}} \right] \quad (18)$$

228 Equation (18) decreases with MLD. As C^* is positive ($C^* \geq 0$) and cannot go to infinity ($C^* \leq$
 229 C_{max}^*), MLD should satisfy $MLD_{C_{max}^*} \leq MLD \leq \frac{\mu^*}{r_{HR} \times K_I^w}$, where $MLD_{C_{max}^*}$ represents the MLD
 230 corresponding to the maximum achievable autotroph's biomass concentration (C_{max}^*) in the
 231 surface ocean. The NCP^* model for $0 \leq MLD < MLD_{C_{max}^*}$ is not discussed here, because we do
 232 not have data with very shallow MLD to constrain and evaluate the model. The derivation of the
 233 model can be found is however presented in the supplementary material. Substituting C^* from
 234 equation (18) into equation (16):

$$235 \quad \sqrt{NCP^*} = a_2 \times \sqrt{-\ln(1 - I_m(0))I_m(0)} + a_1 \times \sqrt{MLD} \quad (19)$$

236 where $a_1 = -\sqrt{\frac{K_I^w \times r_{HR}}{k_c}}$ and $a_2 = \sqrt{\frac{N_m \times \mu_{max}}{k_c}}$. Constants a_1 and a_2 are functions of r_{HR} and μ_{max} ,
 237 respectively, which are generally modeled to increase with temperature (T) (Eppley, 1972; Rivkin
 238 and Legendre, 2001):

$$239 \quad \mu_{max} \propto \mu_{max}^0 \times e^{P_t \times T} \quad (20a)$$

$$240 \quad r_{HR} \propto r_{HR}^0 \times e^{B_t \times T} \quad (20b)$$

241 where P_t and B_t are constants; and μ_{max}^0 and r_{HR}^0 are maximum growth rate and heterotrophic
 242 respiration ratio for $T = 0^\circ\text{C}$, respectively. P_t is commonly assumed to equal 0.0663 (Eppley,
 243 1972). Substituting equations (20a) and (20b) into equation (19) yields:

$$244 \quad \sqrt{NCP^*} = a_4 \times \sqrt{e^{P_t \times T}} \times \sqrt{-\ln(1 - I_m(0))I_m(0)} + a_3 \times \sqrt{e^{B_t \times T}} \times \sqrt{MLD} \quad (21)$$

245 where $a_3 = -\sqrt{\frac{r_{HR}^0 \times K_I^w}{k_c}}$ and $a_4 = \sqrt{\frac{\mu_{max}^0 \times N_m}{k_c}}$. ~~The NCP^* model for $0 \leq MLD < MLD_{C_{max}^*}$ is not~~
 246 ~~discussed here, because we do not have data with very shallow MLD to constrain and evaluate the~~
 247 ~~model. The derivation of the model can be found in the supplementary material.~~

248 2.5. Comparison to observations

249 2.5.1 Data products

250 We assess the performance of our modeled upper bound on carbon export using a global dataset
251 of MLD, PAR, sea surface temperature (SST), O₂/Ar-derived NCP, and export production derived
252 from sediment traps and ²³⁴Th (see supplementary material). MLD was derived from global Argo
253 profiles (Global Ocean Data Assimilation Experiment; <http://www.usgodae.org/>) and CTD casts
254 (National Oceanographic Data Center; <https://www.nodc.noaa.gov/>). PAR was downloaded from
255 the NASA ocean color website (<https://oceancolor.gsfc.nasa.gov/>). The NCP estimates are based
256 on a compilation of O₂/Ar measurements from Li and Cassar (2016), Li et al. (2016), Shadwick et
257 al. (2015), and Martin et al. (2013). The POC export production estimates were obtained from the
258 recently compiled dataset of Mouw et al. (2016). These estimates were adjusted to reflect a flux at
259 the base of mixed layer using the Martin curve of organic carbon attenuation with depth (Martin
260 et al., 1987). The constants k_c and K_I^w in equation (10) were derived assuming a carbon to
261 chlorophyll *a* ratio of 90 (Arrigo et al., 2008) and an empirical linear relationship between K_I and
262 chlorophyll *a* concentration (see Figure S3), calculated based on the NOMAD dataset (Werdell
263 and Bailey, 2005). k_m^l was set at 4.1 Einstein m⁻² d⁻¹ following Behrenfeld and Falkowski (1997).
264 In our estimation of the upper bound on carbon export, we set N_m to 1 in the NCP^* calculations.

265 2.5.2 Results and discussion

266 Overall, we find that NCP^* calculated using published parameters (~~Laws et al., 2000~~[Table 2](#))
267 does a good job of enveloping carbon export observations reported in the literature (Figure [43\(A\)](#)).
268 Samples on the NCP^* envelope (upper bound) are likely regulated by light availability. Conversely,
269 points below the upper bound may be nutrient ~~or in some cases light~~-limited. As expected, NCP^*
270 increases with μ_{max} and decreases with r_{HR} . Model parameters $a_1 = ~~-1.80~~-1.78$ and $a_2 =$
271 ~~21.38~~[14.75](#) (equation (19)) provide the best fit to the [upper bound on](#) O₂/Ar-NCP ~~and as a~~

272 function of MLD. When compared to parameters available in the literature (Table 2), we find
 273 that the best fit to our modeled upper bound is using μ_{max} and r_{HR} of 1.2 d⁻¹ and 0.2 d⁻¹,
 274 respectively. When accounting for the effect of T on μ_{max} and r_{HR} , model constants $a_3 =$
 275 ~~-1.66~~ - 1.53 and $a_4 =$ ~~20.40~~ 13.39 (equation (21)) best fit the upper bound on O₂/Ar-NCP, SST
 276 and MLD observations.

277 Our results show that NCP^* decreases faster with increasing MLD in warmer waters (Figures
 278 43(B) and 4(C)), because the term $a_3 \times \sqrt{e^{B_t \times T}}$ in equation (21) is negative and negatively
 279 correlated to T . This temperature effect contributes to part of the relationship between export
 280 production and MLD in Figure 43(A). Interestingly, NCP^* increases with T in colder waters and
 281 shallow mixed layers (Figure 4(C)). This is because NCP^* reflects the balance between

282 productivity ($a_4 \times \sqrt{e^{P_t \times T}} \times \sqrt{-\ln(1 - I_m(0)) I_{\frac{m}{m}}(\theta)}$) and heterotrophic respiration ($a_3 \times$
 283 $\sqrt{e^{B_t \times T}} \times \sqrt{MLD}$). In a shallow cold mixed layer, the change in productivity with T

284 $\left(\frac{d(a_4 \times \sqrt{e^{P_t \times T}} \times \sqrt{-\ln(1 - I_m(0)) I_{\frac{m}{m}}(\theta)})}{dT} = \frac{P_t}{2} \times a_4 \times \sqrt{e^{P_t \times T}} \times \sqrt{-\ln(1 - I_m(0)) I_{\frac{m}{m}}(\theta)} \right)$ is greater than

285 that of heterotrophic respiration ($\frac{d(a_3 \times \sqrt{e^{B_t \times T}} \times \sqrt{MLD})}{dT} = \frac{B_t}{2} \times a_3 \times \sqrt{e^{B_t \times T}} \times \sqrt{MLD}$). These results

286 could explain part of the variability in the relationship between NCP and SST reported in previous
 287 studies (Li and Cassar, 2016). Our NCP^* model does not perform as well in warmer deep mixed
 288 layers, where high variability in export ratio maxima have also been reported (Cael and Follows,
 289 2016). This may stem from uncertainties in observations, the differing relationship between T ,
 290 μ_{max} , and r_{HR} at high temperature, and/or violations of our assumptions (see caveats and
 291 limitations).

292 Several recent studies have explored the relationship of NCP to oceanic parameters based on
 293 various statistical approaches (Cassar et al., 2015; Chang et al., 2014; Huang et al., 2012; Li and
 294 Cassar, 2016; Li et al., 2016). Our model can shed some light into the mechanisms driving some
 295 of these patterns. To that end, we substitute equation (159) into equation (8):

$$296 \quad NCP(0, MLD) = C \times MLD \times \left(-\frac{N_m \times \mu_{max}}{K_I \times MLD} \times \ln \left(\frac{I_0 \times e^{-K_I \times MLD} + k_m^I}{I_0 + k_m^I} \right) - r_{HR} \right) \quad (22)$$

297 Rearranging equation (22):

$$298 \quad NCP_B = \frac{NCP(0, MLD)}{C \times MLD} = -\frac{\ln \left(\frac{I_0 \times e^{-K_I \times MLD} + k_m^I}{I_0 + k_m^I} \right)}{I_0 \times (1 - e^{-K_I \times MLD})} \times N_m \times \mu_{max} \times PAR_{ML} - r_{HR} \quad (23)$$

299 where NCP_B is the biomass-normalized volumetric NCP, PAR_{ML} is the average PAR in the mixed

300 layer ($PAR_{ML} = \frac{1 - e^{-K_I \times MLD}}{K_I \times MLD} \times I_0$), and $-\frac{\ln \left(\frac{I_0 \times e^{-K_I \times MLD} + k_m^I}{I_0 + k_m^I} \right)}{I_0 \times (1 - e^{-K_I \times MLD})} \frac{1}{I_0 + k_m^I} \times N_m \times \mu_{max}$ and $-r_{HR}$

301 correspond to the slope and offset, respectively. The scatter in the relationship between
 302 chlorophyll-normalized volumetric NCP and PAR_{ML} , as reported in previous studies (Bender et
 303 al., 2016), can likely be explained by the effect of temperature and the availability of nutrient and
 304 light (among other properties) on the slope and offset of equation (23). Equation (22) can also be
 305 reorganized to assess how environmental conditions may impact the export ratio (ef):

$$306 \quad ef = \frac{NCP(0, MLD)}{NPP(0, MLD)} = 1 - \frac{K_I \times MLD}{-\ln \left(\frac{I_0 \times e^{-K_I \times MLD} + k_m^I}{I_0 + k_m^I} \right)} \times \frac{1}{N_m} \times \frac{r_{HR}}{\mu_{max}} \quad (24)$$

307 where $\frac{r_{HR}}{\mu_{max}}$ is proportional to $e^{(B_t - P_t) \times T}$. Equation (24) is consistent with multiple studies which
 308 predict decreasing ef with increasing temperature (Cael and Follows, 2016; Dunne et al., 2005;
 309 Henson et al., 2011; Laws et al., 2000; Li and Cassar, 2016). In fact, equation (5) of Cael and
 310 Follows (2016) can easily be derived from equation (24) (see supplementary material). Equation

311 (24) also highlights that a multitude of factors may confound the dependence of ef on temperature
312 (including varying MLD, light attenuation, and availability of nutrient and light). This again may
313 explain some of the conflicting observations recently reported in the literature (e.g., Maiti et al.
314 (2013)), where the effect of temperature may be masked by changes in community composition
315 (Britten et al., 2017; Henson et al., 2015). One therefore needs to account or correct for the
316 multitude of confounding factors when predicting the effect of a given environmental condition
317 (e.g., temperature, mineral ballast, and NPP) on the export ratio.

318 **3. Spatial distribution of the upper bound on carbon export**

319 We estimate the global distribution of the upper bound of carbon export using equation (19)
320 and climatological monthly MLD and PAR. In general, NCP^* is high in low latitudes and low in
321 the North Atlantic and Antarctic Circumpolar Current (ACC) in the Southern Ocean (Figure
322 [54\(A\)](#)). As expected, this spatial pattern is controlled by MLD (see Figure S1). Satellite-derived
323 estimates of NCP (Li and Cassar, 2016) are approximately 10% of global NCP^* , reflecting the
324 high degree of nutrient limitation in the oceans. We also derive a global NCP^* map using equation
325 (21), and find that the global NCP^* estimate is very sensitive to the temperature dependence of
326 r_{HR} . For example, decreasing the B_t in $r_{HR} = r_{HR}^0 \times e^{B_t \times T}$ from 0.11 to 0.08 (as used in Rivkin
327 and Legendre (2001) and López-Urrutia et al. (2006)) increases the global NCP^* budget by a factor
328 of 2.4. Large differences in NCP^* in low-latitudes in great part explain this change. In light of the
329 large uncertainties in the relationship between r_{HR} and T (Cael and Follows, 2016; López-Urrutia
330 et al., 2006), we hereafter only discuss NCP^* estimates derived from equation (19).

331 To estimate how close export production is to its upper bound, we calculate the ratio of export
332 production to NCP^* (f_{pt}). Low f_{pt} regimes represent ecosystems likely regulated by nutrient
333 availability (i.e., ecosystems that have not reached their full export potential based on MLD and

334 [surface PAR](#)). As expected, low latitude and subtropical regions have low f_{pt} (Figure [54\(B\)](#)). High
335 f_{pt} regimes represent ecosystems which have reached their full light potential, and are therefore
336 less likely to respond to nutrient addition because of light limitation (e.g., North Atlantic and ACC
337 (Figure [54\(B\)](#))). In these regions, especially the subantarctic region, f_{pt} is high in the spring
338 (Figure [54\(C\)](#)) and decreases in the summer (Figure [54\(D\)](#)), suggesting that export production is
339 likely co-limited by nutrient and light availability. This may in part explain the lower response to
340 iron fertilization in the subantarctic region where substantial increases in surface chlorophyll were
341 only observed in regions with shallower mixed layers (Boyd et al., 2007; Boyd et al., 2000; de
342 Baar et al., 2005).

343 Also shown in Figure [54](#) are the biological pump efficiency and export ratio ef (panels [54E](#)
344 and [54F](#), respectively). These various proxies reflect different components of the biological pump.
345 Whereas f_{pt} reflects the export potential based on current MLD and light availability, the
346 biological pump efficiency reflects the potential as derived from nutrient distribution in the oceans,
347 estimated from the extent of nutrient removal from the surface ocean (Sarmiento and Gruber, 2006)
348 or the proportion of regenerated nutrients at depth (Ito and Follows, 2005). A revised estimate of
349 the global biological pump efficiency, estimated based on the proportion of regenerated to total
350 nutrients (preformed + regenerated) at depth is around 30-35% (Duteil et al., 2013). The ef ratio
351 on the other hand describes how much of production is exported as opposed to recycled in the
352 surface (Dunne et al., 2005). The ultra-oligotrophic subtropical waters have a low export ratio, a
353 strong biological pump efficiency with exhaustion of nutrients at the ocean surface, and therefore
354 have not reached their full light potential (low f_{pt}) because of the strong stratification and nutrient
355 limitation. The seasonal pattern of f_{pt} in the subantarctic region suggests that the low biological

356 pump efficiency is the result of light limitation in the austral spring and nutrient (likely Fe) and
357 light limitation in the austral summer.

358 4. Caveats and limitations

359 ~~A-There are a~~ multitude of uncertainties, simplifications, and approximations in our model and
360 field observations ~~may explain some of the discrepancies between the predicted and observed~~

361 ~~NCP*~~. Among others:

362 • In our study, we used a model which builds on Sverdrup’s critical depth hypothesis. There
363 are competing hypotheses to explain phytoplankton bloom phenology (timing and
364 intensity), including the “dilution recoupling hypothesis” or “disturbance recovery
365 hypothesis” (Behrenfeld, 2010; Boss and Behrenfeld, 2010) and “critical turbulence
366 hypothesis” (Brody and Lozier, 2015; Huisman et al., 1999; Taylor and Ferrari, 2011). In
367 the case of top-down control, any respiratory grazing loss not accounted for by our loss
368 term would behave as a system not reaching its full light potential (NCP*). Conversely,
369 any grazing loss associated with export (e.g., rapidly sinking fecal pellets and other
370 zooplankton-mediated export pathways) would minimize respiratory losses thereby
371 bringing NCP closer to its upper bound based on light-availability. These opposing effects
372 are beyond the scope of this study, but could be modeled, especially as we learn more about
373 their impacts on carbon fluxes through new efforts such as NASA’s EXPORTS program
374 (Siegel et al., 2016). See also the point below on mixing vs. mixed layer depth.

375 • Phytoplankton biomass concentration (C) may vary with depth in the mixed layer,
376 especially for water columns experiencing varying degrees of turbulent mixing. In addition,
377 MLD is not always the best proxy of light availability with mixing layer in some cases

378 deviating from the mixed layer (Franks, 2015; Huisman et al., 1999). The factors defining
379 the MLD also vary in different oceanic regions.

380 • For simplicity, we model the dependence of photosynthesis on irradiance assuming
381 Michaelis-Menten kinetics, which does not account for photoinhibition. More accurate
382 models can be found in other studies (Platt et al., 1980). Due to optional absorption, K_I
383 also varies with depth in the mixed layer. Additionally, the linear relationship between K_I
384 and C is influenced by CDOM, NAP, and other environmental factors (e.g., solar zenith
385 angle) (Gordon, 1989).

386 • μ_{max} and r_{HR} are influenced by environmental factors other than temperature, including
387 community structure (Chen and Laws, 2017), and may vary with depth within the mixed
388 layer (Smetacek and Passow, 1990). For these reasons, the equations relating μ_{max} and r_{HR}
389 (i.e., B_t and P_t) to temperature also carry significant uncertainties (Bissinger et al., 2008;
390 Edwards et al., 2016; Kremer et al., 2017; López-Urrutia and Morán, 2007; Rivkin and
391 Legendre, 2001) which impacts our estimates of the upper bound on carbon export,
392 especially in warmer regions. As in other recent studies (Cael and Follows, 2016; Cael et
393 al., 2017; Dutkiewicz et al., 2001; Gong et al., 2015; Gong et al., 2017; Huisman et al.,
394 2006; Taylor and Ferrari, 2011), we model heterotrophic respiration to vary in proportion
395 to phytoplankton concentration. The model could be further improved by explicitly
396 including the concentration of heterotrophs. See point above on the grazing effect on export
397 with regards to r_{HR} .

398 • NCP may underestimate export production when accompanied by a decrease in the
399 inventory of organic matter in the mixed layer (see introduction and equation (2)).

- 400 • Our field observations are limited, mostly focusing on the spring and summer seasons, and
401 harbor significant uncertainties. For example, deep mixed layers can bias the O₂/Ar method
402 low if entrainment of deeper waters brings low O₂ into the mixed layer. Descriptions of
403 these uncertainties are presented in other studies (Bender et al., 2011; Cassar et al., 2014;
404 Jonsson et al., 2013).
- 405 • Finally, our study is only relevant to the mixed layer. It does not account for productivity
406 below the mixed layer, which can be important in some regions such as the subtropical
407 ocean.

408 **5. Conclusions**

409 In this study, we derived a mechanistic model of an upper bound on carbon export (*NCP**) based
410 on the metabolic balance between photosynthesis and respiration of the plankton community. The
411 upper bound is a positively skewed bell-shaped function of mixed layer depth (MLD). At low
412 temperatures, the upper bound decreases with temperature if mixed layers are deep, but increases
413 with temperature if mixed layers are shallow. We used this model to derive a global distribution
414 of an upper bound on carbon export as a function of MLD and surface PAR, which shows high
415 values in low latitudes and low values in high latitudes due to deep MLD. To examine how current
416 export production compares to this upper bound in the world's oceans, we calculated the ratio of
417 satellite export production estimates to the upper bound derived by our model. High ratios of export
418 production to *NCP** in the North Atlantic and ACC indicate that export production in these regions
419 is likely co-limited by nutrient and light availability. Overall, our results may explain differences
420 in carbon export measured during past iron fertilization experiments (e.g., subantarctic and polar
421 regions), inform future iron fertilization experiments, ~~and~~ help in the development of remotely-

422 sensed carbon export [algorithms, and improve predictions of the response of marine ecosystems](#)
423 [to a changing climate](#).

424 **Acknowledgements**

425 We would like to acknowledge NASA GSFC for processing and distributing PAR and SST
426 products (<http://oceancolor.gsfc.nasa.gov/>). Global Argo temperature-salinity profiling floats were
427 downloaded from <http://www.usgoda.org/>. CTD casts were downloaded from National
428 Oceanographic Data Center (<https://www.nodc.noaa.gov/>). N.C. was supported by NSF OPP-
429 1043339. Z.L. was supported by a NASA Earth and Space Science Fellowship (Grant No.
430 NNX13AN85H). [The authors thank three anonymous reviewers for their insightful comments.](#)

431 **References**

- 432 Arrigo, K. R., van Dijken, G. L., and Bushinsky, S.: Primary production in the Southern Ocean,
433 1997-2006, *J. Geophys. Res.*, 113, doi:10.1029/2007JC004551, 2008.
- 434 Baker, K. S. and Smith, R. C.: Bio-optical classification and model of natural-waters .2, *Limnol.*
435 *and Oceanogr.*, 27, 500-509, doi:10.4319/lo.1982.27.3.0500, 1982.
- 436 Behrenfeld, M. J.: Abandoning Sverdrup's Critical Depth Hypothesis on phytoplankton blooms,
437 *Ecology*, 91, 977–989, doi:10.1890/09-1207.1, 2010.
- 438 Behrenfeld, M. J. and Falkowski, P. G.: Photosynthetic rates derived from satellite-based
439 chlorophyll concentration, *Limnol. and Oceanogr.*, 42, 1-20,
440 doi:10.4319/lo.1997.42.1.0001, 1997.
- 441 Bender, M. L., Tilbrook, B., Cassar, N., Jonsson, B. F., Poisson, A., and Trull, T. W.: Ocean
442 productivity south of Australia during spring and summer, *Deep-Sea Res. Pt. I*, 112, 68-78,
443 doi:10.1016/j.dsr.2016.02.018, 2016.
- 444 Bender, M. L., Kinter, S., Cassar, N., and Wanninkhof, R.: Evaluating gas transfer velocity
445 parameterizations using upper ocean radon distributions, *J. Geophys. Res.*, 116,
446 doi:10.1029/2009JC005805, 2011.
- 447 Bissinger, J. E., Montagnes, D. J. S., Sharples, J., and Atkinson, D.: Predicting marine
448 phytoplankton maximum growth rates from temperature: Improving on the Eppley curve

449 using quantile regression, *Limnol. Oceanogr.*, 53, 487–493,
450 doi:10.4319/lo.2008.53.2.0487, 2008.

451 Boss, E. and Behrenfeld, M. J.: In situ evaluation of the initiation of the North Atlantic
452 phytoplankton bloom, *Geophys. Res. Lett.*, 37, doi:10.1029/2010GL044174, 2010.

453 Boyd, P. W., Jickells, T., Law, C. S., Blain, S., Boyle, E. A., Buesseler, K. O., Coale, K. H., Cullen,
454 J. J., de Baar, H. J. W., Follows, M., Harvey, M., Lancelot, C., Levasseur, M., Owens, N.
455 P. J., Pollard, R., Rivkin, R. B., Sarmiento, J., Schoemann, V., Smetacek, V., Takeda, S.,
456 Tsuda, A., Turner, S., and Watson, A. J.: Mesoscale iron enrichment experiments 1993-
457 2005: Synthesis and future directions, *Science*, 315, 612-617,
458 doi:10.1126/science.1131669, 2007.

459 Boyd, P. W., Watson, A. J., Law, C. S., Abraham, E. R., Trull, T., Murdoch, R., Bakker, D. C. E.,
460 Bowie, A. R., Buesseler, K. O., Chang, H., Charette, M., Croot, P., Downing, K., Frew, R.,
461 Gall, M., Hadfield, M., Hall, J., Harvey, M., Jameson, G., LaRoche, J., Liddicoat, M., Ling,
462 R., Maldonado, M. T., McKay, R. M., Nodder, S., Pickmere, S., Pridmore, R., Rintoul, S.,
463 Safi, K., Sutton, P., Strzepek, R., Tanneberger, K., Turner, S., Waite, A., and Zeldis, J.: A
464 mesoscale phytoplankton bloom in the polar Southern Ocean stimulated by iron
465 fertilization, *Nature*, 407, 695-702, doi:10.1038/35037500, 2000.

466 Britten, G. L., Wakamatsu, L., and Primeau, F. W.: The temperature-ballast hypothesis explains
467 carbon export efficiency observations in the Southern Ocean, *Geophys. Res. Lett.*, 44,
468 1831-1838, doi:10.1002/2016GL072378, 2017.

469 Brody, S. R. and Lozier, M. S.: Characterizing upper-ocean mixing and its effect on the spring
470 phytoplankton bloom with in situ data, *ICES J. Mar. Sci.*, 72, 1961–1970.
471 doi:10.1093/icesjms/fsv006, 2015

472 Cael B. B., Bisson, K., and Follows, M. J.: How have recent temperature changes affected the
473 efficiency of ocean biological carbon export? *Limnology and Oceanography Letters*, 2,
474 113-118, doi:10.1002/lo12.10042, 2017.

475 Cael, B. B. and Follows, M. J.: On the temperature dependence of oceanic export efficiency,
476 *Geophys. Res. Lett.*, 43, 5170-5175, doi:10.1002/2016GL068877, 2016.

477 Cassar, N., Nevison, C. D., and Manizza, M.: Correcting oceanic O₂/Ar-net community production
478 estimates for vertical mixing using N₂O observations, *Geophys. Res. Lett.*, 41, 8961-8970,
479 doi:10.1002/2014GL062040, 2014.

480 Cassar, N., DiFiore, P. J., Barnett, B. A., Bender, M. L., Bowie, A. R., Tilbrook, B., Petrou, K.,
481 Westwood, K. J., Wright, S. W., and Lefevre, D.: The influence of iron and light on net
482 community production in the Subantarctic and Polar Frontal Zones, *Biogeosciences*, 8,
483 227-237, doi:10.5194/bg-8-227-2011, 2011.

484 Cassar, N., Wright, S. W., Thomson, P. G., Trull, W. T., Westwood, K. J., de Salas, M., Davidson,
485 A., Pearce, I., Davies, D. M., and Matear, R. J.: The relation of mixed-layer net community
486 production to phytoplankton community composition in the Southern Ocean, *Global
487 Biogeochem. Cy.*, 29, 446-462, doi:10.1002/2014GB004936, 2015.

488 Chang, C.-H., Johnson, N. C., and Cassar, N.: Neural network-based estimates of Southern Ocean
489 net community production from in situ O₂/Ar and satellite observation: a methodological
490 study, *Biogeosciences*, 11, 3279-3297, <https://doi.org/10.5194/bg-11-3279-2014>, 2014.

491 Chen, B., Laws, E. A.: Is there a difference of temperature sensitivity between marine
492 phytoplankton and heterotrophs? *Limnol. and Oceanogr.*, 62, 806-817,
493 doi:10.1002/lno.10462, 2017.

494 Cullen, J. J. and Lewis, M. R.: The kinetics of algal photoadaptation in the context of vertical
495 mixing, *J. Plankton Res.*, 10, 1039-1063, doi:10.1093/plankt/10.5.1039, 1988.

496 de Barr, J. W. H., Boyd, P. W., Coale, K. H., Landry M. R., Tsuda, A., Assmy, P., Bakker, D. C.
497 E., Bozec, Y., Barber, R. T., Brzezinski, M. A., Buesseler, K. O., Boyé, M., Croot, P. L.,
498 Gervais, F., Gorbunov, M. Y., Harrison, P. J., Hiscock, W. T., Laan, P., Lancelot, C., Law,
499 C. S., Levasseur, M., Marchetti, A., Millero, F. J., Nishioka, J., Nojiri, Y., van Oijen, T.,
500 Riebesell, U., Rijkenberg, M. J. A., Saito, H., Takeda, S., Timmermans, K. R., Veldhuis,
501 M. J. W., Waite, A. M., and Wong, C. S.: Synthesis of iron fertilization experiments: From
502 the Iron age in the Age of Enlightenment, *J. Geophys. Res.*, 110, C09S16,
503 doi:10.1029/2004JC002601, 2005.

504 Dunne, J. P., Armstrong, R. A., Gnanadesikan, A., and Sarmiento, J. L.: Empirical and mechanistic
505 models for the particle export ratio, *Global Biogeochem. Cy.*, 19,
506 doi:10.1029/2004GB002390, 2005.

507 Duteil, O., Koeve, W., Oschlies, A., Bianchi, D., Galbraith, E., Kriest, I., and Matear, R.: A novel
508 estimate of ocean oxygen utilisation points to a reduced rate of respiration in the ocean
509 interior, *Biogeosciences*, 10, 7723-7738, <https://doi.org/10.5194/bg-10-7723-2013>, 2013.

510 Dutkiewicz, S., Follows, M., Marshall, J., and Gregg, W. W.: Interannual variability of
511 phytoplankton abundances in the North Atlantic, *Deep-Sea Res. Pt. II*, 48, 2323-2344,
512 doi:10.1016/S0967-0645(00)00178-8, 2001.

513 Edwards, K. F., Thomas, M. K., Klausmeier, C. A., and Litchman, E.: Phytoplankton growth and
514 the interaction of light and temperature: A synthesis at the species and community
515 level, *Limnol. and Oceanogr.*, 61, 1232–1244, doi:10.1002/lno.10282, 2016.

516 Eppley, R. W.: Temperature and phytoplankton growth in the sea, *Fishery Bulletin*, 70, 1063-1085,
517 1972.

518 Eveleth, R., Cassar, N., Sherrell, R. M., Ducklow, H., Meredith, M., Venables, H., Lin, Y., and Li,
519 Z.: Ice melt influence on summertime net community production along the Western
520 Antarctic Peninsula, *Deep-Sea Res. Pr. II*, 139, 89-102, doi:10.1016/j.dsr2.2016.07.016,
521 2017.

522 Falkowski, P. G., Barber, R. T., and Smetacek, V.: Biogeochemical controls and feedbacks on
523 ocean primary production, *Science*, 281, 200-206, doi:10.1126/science.281.5374.200,
524 1998.

525 Franks, P. J. S.: Has Sverdrup's critical depth hypothesis been tested? Mixed layers vs. turbulent
526 layers, *ICES J. Mar. Sci.*, 72, 1897-1907, doi:10.1093/icesjms/fsu175, 2015.

527 [Gong, X., Shi, J., Gao, H. W., and Yao, X. H.: Steady-state solutions for subsurface chlorophyll](#)
528 [maximum in stratified water columns with a bell-shaped vertical profile of chlorophyll,](#)
529 [Biogeosciences, 12, 905-919, doi:10.5194/bg-12-905-2015, 2015.](#)

530 [Gong, X., Jiang, W., Wang, L., Gao, H., Boss, E., Yao, X., Kao, S., and Shi, J.: Analytical solution](#)
531 [of the nitracline with the evolution of subsurface chlorophyll maximum in stratified water](#)
532 [columns, Biogeosciences, 14, 2371-2386, doi:10.5194/bg-14-2371-2017, 2017.](#)

533 Gordon, H. R.: Can the Lambert-Beer law be applied to the diffuse attenuation coefficient of ocean
534 water, *Limnol. and Oceanogr.*, 34, 1389-1409, doi:10.4319/lo.1989.34.8.1389, 1989.

535 Henson, S. A., Yool, A., and Sanders, R.: Variability in efficiency of particulate organic carbon
536 export: A model study, *Global Biogeochem. Cy.*, 29, 33-45, doi:10.1002/2014GB004965,
537 2015.

538 Henson, S. A., Sanders, R., Madsen, E., Morris, P. J., Le Moigne, F., and Quartly, G. D.: A reduced
539 estimate of the strength of the ocean's biological carbon pump, *Geophys. Res. Lett.*, 38,
540 L04606, doi:10.1029/2011GL046735, 2011.

541 Huang, K., Ducklow, H., Vernet, M., Cassar, N., and Bender, M. L.: Export production and its
542 regulating factors in the West Antarctica Peninsula region of the Southern Ocean, *Global*
543 *Biogeochem. Cy.*, 26, GB2005, doi:10.1029/2010GB004028, 2012.

544 Huisman, J. and Weissing, F. J.: Light-limited growth and competition for light in well-mixed
545 aquatic environments: An elementary model, *Ecology*, 75, 507-520, doi:10.2307/1939554,
546 1994.

547 Huisman, J., van Oostveen, P., and Weissing, F. J.: Critical depth and critical turbulence: Two
548 different mechanisms for the development of phytoplankton blooms, *Limnol. and*
549 *Oceanogr.*, 44, 1781-1787, doi:10.4319/lo.1999.44.7.1781, 1999.

550 [Huisman, J., Thi, N. N. P., Karl, D. M., and Sommeijer B.: Reduced mixing generates oscillations](#)
551 [and chaos in the oceanic deep chlorophyll maximum, *Nature*, 439, 322-325,](#)
552 [doi:10.1038/nature04245, 2006.](#)

553 Ito, T., and Follows, M. J.: Preformed phosphate, soft tissue pump and atmospheric CO₂, *J. Mar.*
554 *Res.*, 63, 813-839, doi:10.1357/0022240054663231, 2005.

555 Jonsson, B. F., Doney, S. C., Dunne, J., and Bender, M.: Evaluation of the Southern Ocean O₂/Ar-
556 based NCP estimates in a model framework, *J. Geophys. Res.*, 118, 385-399,
557 doi:10.1002/jgrg.20032, 2013.

558 Kremer, C. T., Thomas, M. K., and Litchman, E.: Temperature- and size-scaling of phytoplankton
559 population growth rates: Reconciling the Eppley curve and the metabolic theory of ecology,
560 *Limnol. and Oceanogr.*, 62, 1658-1670, doi:10.1002/lno.10523, 2017.

561 Laws, E. A., Falkowski, P. G., Smith, W. O., Ducklow, H., and McCarthy, J. J.: Temperature
562 effects on export production in the open ocean, *Global Biogeochem. Cy.*, 14, 1231-1246,
563 doi:10.1029/1999GB001229, 2000.

564 Lewis, M. R., Cullen, J. J., and Platt, T.: Relationships between vertical mixing and
565 photoadaptation of phytoplankton: Similarity criteria, *Mar. Ecol. Prog. Ser.*, 15, 141-149,
566 doi:10.3354/meps015141, 1984.

567 Li, Z. and Cassar, N.: Satellite estimates of net community production based on O₂/Ar observations
568 and comparison to other estimates, *Global Biogeochem. Cy.*, 30, 735-752,
569 doi:10.1002/2015GB005314, 2016.

570 Li, Z., Cassar, N., Huang, K., Ducklow, H., and Schofield, O.: Interannual variability in net
571 community production at the Western Antarctic Peninsula region (1997-2014), *J. Geophys.*
572 *Res.*, 121, 4748-4762, doi:10.1002/2015JC011378, 2016.

573 López-Urrutia, A. and Morán, X. A. G.: Resource limitation of bacterial production distorts the
574 temperature dependence of oceanic carbon cycling, *Ecology*, 88, 817–822,
575 doi:10.1890/06-1641, 2007.

576 López-Urrutia, Á., San Martín, E., Harris, R. P., and Irigoien, X.: Scaling the metabolic balance
577 of the oceans, *Proc. Natl Acad. Sci. USA*, 103, 8739-8744, doi:10.1073/pnas.0601137103,
578 2006.

579 Maiti, K., Charette, M. A., Buesseler, K. O., and Kahru M.: An inverse relationship between
580 production and export efficiency in the Southern Ocean, *Geophys. Res. Lett.*, 40, 1557-
581 1561, doi:10.1002/grl.50219, 2013.

582 Martin, J. H., Knauer, G. A., Karl, D. M., and Broenkow, W. W.: VERTEX: carbon cycling in the
583 northeast Pacific, *Deep-Sea Res. Pr. A*, 34, 267-285, doi:10.1016/0198-0149(87)90086-0,
584 1987.

585 Martin, P., Rutgers van der Loeff, M., Cassar, N., Vandromme, P., d'Ovidio, F., Stemman, L.,
586 Rengarajan, R., Soares, M., Gonzalez, H. E., Ebersbach, F., Lampitt, R., Sanders, R.,
587 Barnett, B., Smetacek, V., and Naqvi, S. W. A.: Iron fertilization enhanced net community
588 production but not downward particle flux during the Southern Ocean iron fertilization
589 experiment LOHAFEX, *Global Biogeochem. Cy.*, 27, 871–881, doi:10.1002/gbc.20077,
590 2013.

591 Mitchell, B. G. and Holm-Hansen, O.: Observations and modeling of the Antarctic phytoplankton
592 crop in relation to mixing depth, *Deep-Sea Res. Pr. A*, 38, 981-1007, doi:10.1016/0198-
593 0149(91)90093-U, 1991.

594 Mitchell, B. G., Brody, E. A., Holm-Hansen, O., McClain, C., and Bishop, J.: Light limitation of
595 phytoplankton biomass and macronutrient utilization in the Southern Ocean, *Limnol. and*
596 *Oceanogr.*, 36, 1662-1677, doi:10.4319/lo.1991.36.8.1662, 1991.

597 Morel, A. and Prieur, L.: Analysis of variations in ocean color, *Limnol. and Oceanogr.*, 22, 709-
598 722, doi:10.4319/lo.1977.22.4.0709, 1977.

599 Mouw, C. B., Barnett, A., McKinley, G., Gloege, L., and Pilcher, D.: Global ocean particulate
600 organic carbon flux merged with satellite parameters, *Earth Syst. Sci. Data*, 8, 531-541,
601 doi:10.5194/essd-8-531-2016, 2016.

602 [Nelson, D. M. and Smith, W. O.: Sverdrup revisited: Critical depths, maximum chlorophyll levels,
603 and the control of Southern Ocean productivity by the irradiance-mixing regime, *Limnol.
604 and Oceanogr.*, 36, 1650-1661, doi:10.4319/lo.1991.36.8.1650, 1991.](#)

605 Platt, T., Gallegos, C. L., and Harrison, W. G.: Photoinhibition of photosynthesis in natural
606 assemblages of marine phytoplankton, *J. Mar. Res.*, 38, 687-701, 1980.

607 Rivkin, R. B. and Legendre, L.: Biogenic carbon cycling in the upper ocean: Effects of microbial
608 respiration, *Science*, 291, 2398-2400, doi:10.1126/science.291.5512.2398, 2001.

609 Sarmiento, J. L. and Gruber, N.: *Ocean Biogeochemical Dynamics*, Princeton University Press,
610 Princeton, New Jersey, 2006.

611 Shadwick, E. H., Tilbrook, B., Cassar, N., Trull, T. W., and Rintoul, S. R.: Summertime physical
612 and biological controls on O₂ and CO₂ in the Australian Sector of the Southern Ocean, *J.
613 Marine Syst.*, 147, 21-28, doi:10.1016/j.jmarsys.2013.12.008, 2015.

614 Siegel, D. A., Buesseler, K. O., Behrenfeld, M. J., Benitez-Nelson, C. R., Boss, E., Brzezinski, M.
615 A., Burd, A., Carlson, C. A., D'Asaro, E. A., Doney, S. C., Perry, M. J., Stanley, R. H. R.,
616 and Steinberg, D. K.: Prediction of the export and fate of global ocean net primary
617 production: The exports science plan, *Front. Mar. Sci.*, 3, doi:10.3389/fmars.2016.00022,
618 2016.

619 Sigman, D. M. and Boyle, E. A.: Glacial/interglacial variations in atmospheric carbon dioxide,
620 *Nature*, 407, 859-869, doi:10.1038/35038000, 2000.

621 Smetacek, V. and Passow, U.: Spring bloom initiation and Sverdrup's critical depth model, *Limnol.
622 and Oceanogr.*, 35, 228-234, doi:10.4319/lo.1990.35.1.0228, 1990.

623 Smith, R. C. and Baker, K. S.: Optical classification of natural waters, *Limnol. and Oceanogr.*, 23,
624 260-267, doi:10.4319/lo.1978.23.2.0260, 1978a.

625 Smith, R. C. and Baker, K. S.: The bio-optical state of ocean waters and remote sensing, *Limnol.
626 and Oceanogr.*, 23, 247-259, doi:10.4319/lo.1978.23.2.0247, 1978b.

627 Stange, P., Bach, L. T., Le Moigne, F. A. C., Taucher, J., Boxhammer, T., and Riebesell, U.:
628 Quantifying the time lag between organic matter production and export in the surface ocean:

629 Implications for estimates of export efficiency, *Geophys. Res. Lett.*, 44, 268-276,
630 doi:10.1002/2016GL07087, 2017.

631 Sunda, W. G. and Huntsman, S. A.: Interrelated influence of iron, light and cell size on marine
632 phytoplankton growth, *Nature*, 390, 389-392, doi:10.1038/37093, 1997.

633 Sverdrup, H. U., On conditions for the vernal blooming of phytoplankton, *Journal du Conseil*
634 *International pour l'Exploration de la Mer*, 18, 287-295, doi:10.1093/icesjms/18.3.287,
635 1953.

636 Taylor, J. R. and Ferrari, R.: Shutdown of turbulent convection as a new criterion for the onset of
637 spring phytoplankton blooms, *Limnol. And Oceanogr.*, 56, 2293-
638 2307, doi:10.4319/lo.2011.56.6.2293, 2011.

639 Tortell, P. D., Bittig, H. C., Körtzinger, A., Jones, E. M., and Hoppema, M.: Biological and
640 physical controls on N₂, O₂, and CO₂ distributions in contrasting Southern Ocean surface
641 waters, *Global Biogeochem. Cy.*, 29, 994-1013, doi:10.1002/2014GB004975, 2015.

642 Volk, T. and Hoffert, M. I.: Ocean carbon pumps: Analysis of relative strengths and efficiencies
643 in ocean-driven atmospheric CO₂ changes, in: *The Carbon Cycle and Atmospheric CO₂:
644 Natural Variations Archean to Present*, *Geophys. Monogr. Ser.*, Vol. 32, edited by
645 Sundquist, E. T. and Broecker, W. S., AGU, Washington, D. C., 99-110, 1985.

646 Werdell, P. J. and Bailey, S. W.: An improved in-situ bio-optical data set for ocean color algorithm
647 development and satellite data product validation, *Remote Sensing of Environment*, 98,
648 122-140, doi:10.1016/j.rse.2005.07.001, 2005.

649 White, P. A., Kalff, J., Rasmussen, J. B., and Gasol, J. M.: The effect of temperature and algal
650 biomass on bacterial production and specific growth rate in fresh water and marine habitats,
651 *Microb. Ecol.*, 21, 99-118, 1991.

652

653

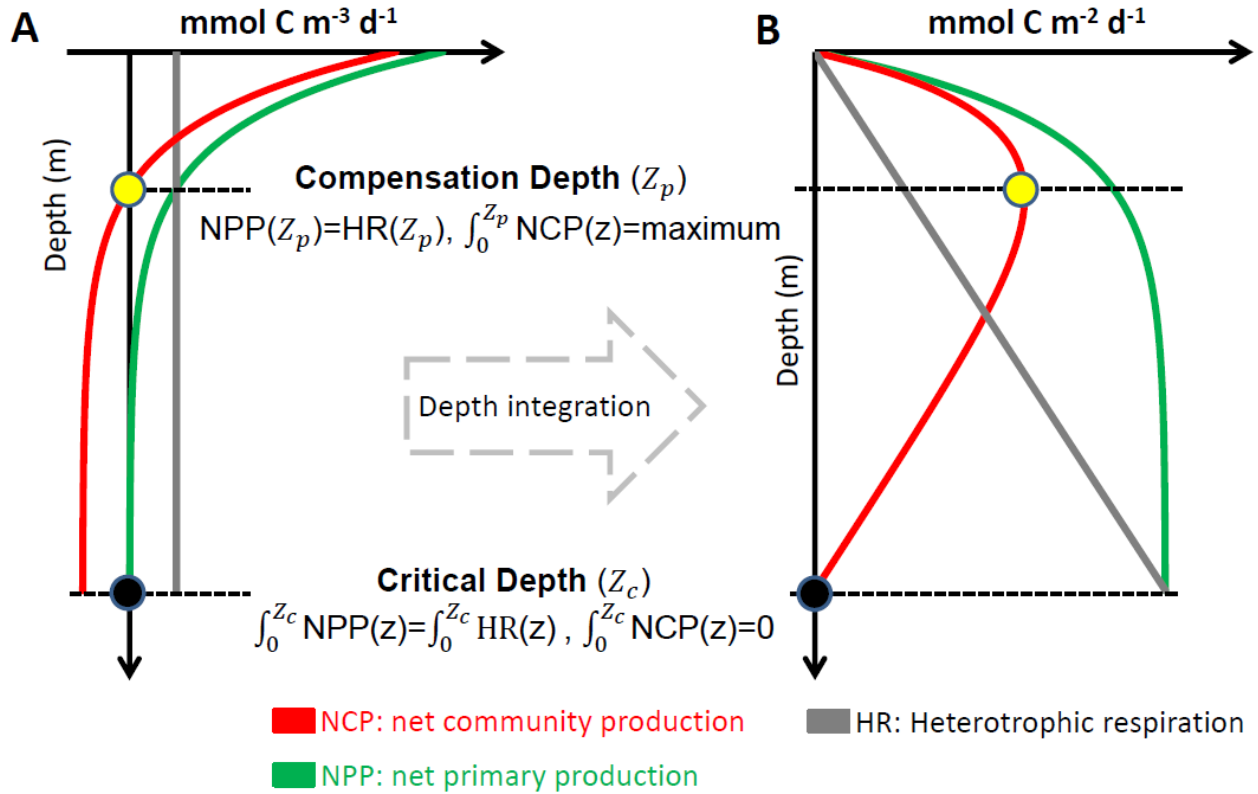


Figure 1. Schematic diagram of depth-profiles of net community production (NCP), net primary production (NPP), and heterotrophic respiration (HR). Yellow and black dots represent the compensation and critical depths, respectively.

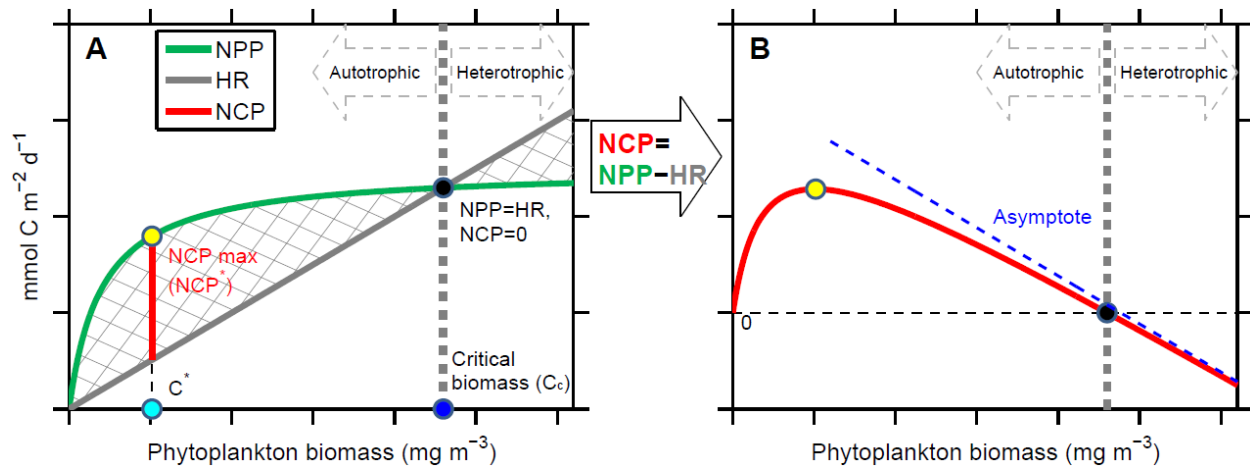


Figure 2. Relationship between net primary production (NPP), heterotrophic respiration (HR), net community production (NCP), and phytoplankton biomass concentration (C) for a given mixed layer depth (MLD). Hatched area in panel A represents NCP. The yellow dot represents the maximal NCP (NCP^*) obtainable for a given MLD, with the corresponding phytoplankton biomass concentration (C^*) denoted with a cyan dot. NCP on the right of the yellow dot decreases with C due to self-shading. Black dot represents depth-integrated $\text{NCP} = 0$ (i.e., $\text{NPP} = \text{HR}$), with the corresponding phytoplankton biomass concentration defined as critical biomass (C_c) and denoted with a blue dot. Ecosystems on the left and right of this threshold are net autotrophic and heterotrophic, respectively. The asymptote (dashed blue line) in panel B represents a system dominated by heterotrophic respiration (i.e., $\text{NCP} \approx \text{HR} \gg \text{NPP}$).

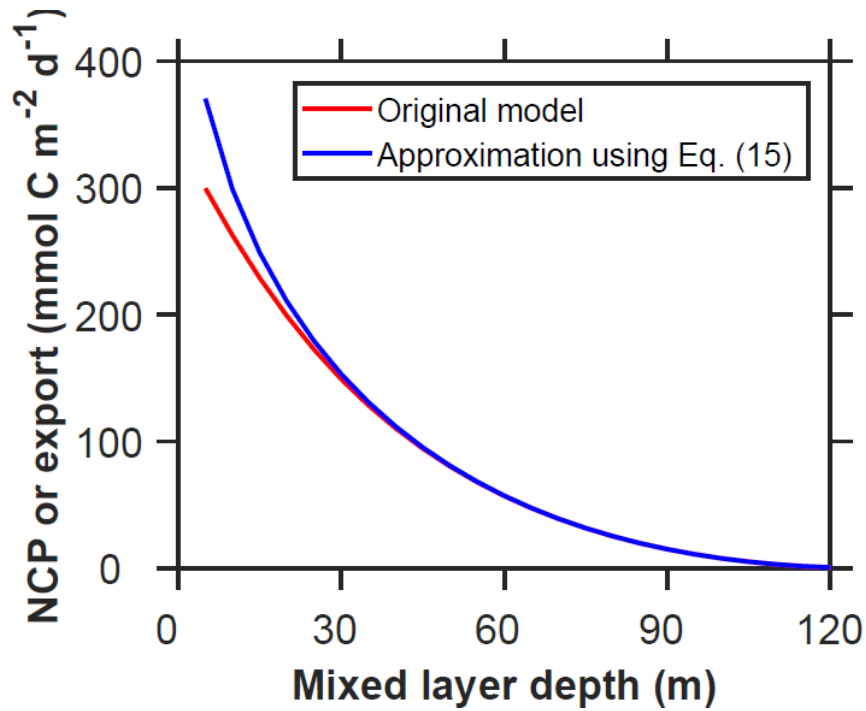


Figure 3. Upper bounds derived using the original and approximated models. The upper bound for the original model (equations (8-10)) is estimated through a non-linear optimization approach. The upper bound for the approximated model is calculated analytically from equation (19). The models use the constants listed in Table 2 and $I_m(0) = 0.9$. Decreasing $I_m(0)$ and increasing r_{HR} results in greater discrepancies between the original and approximated models in regions with shallow mixed layers.

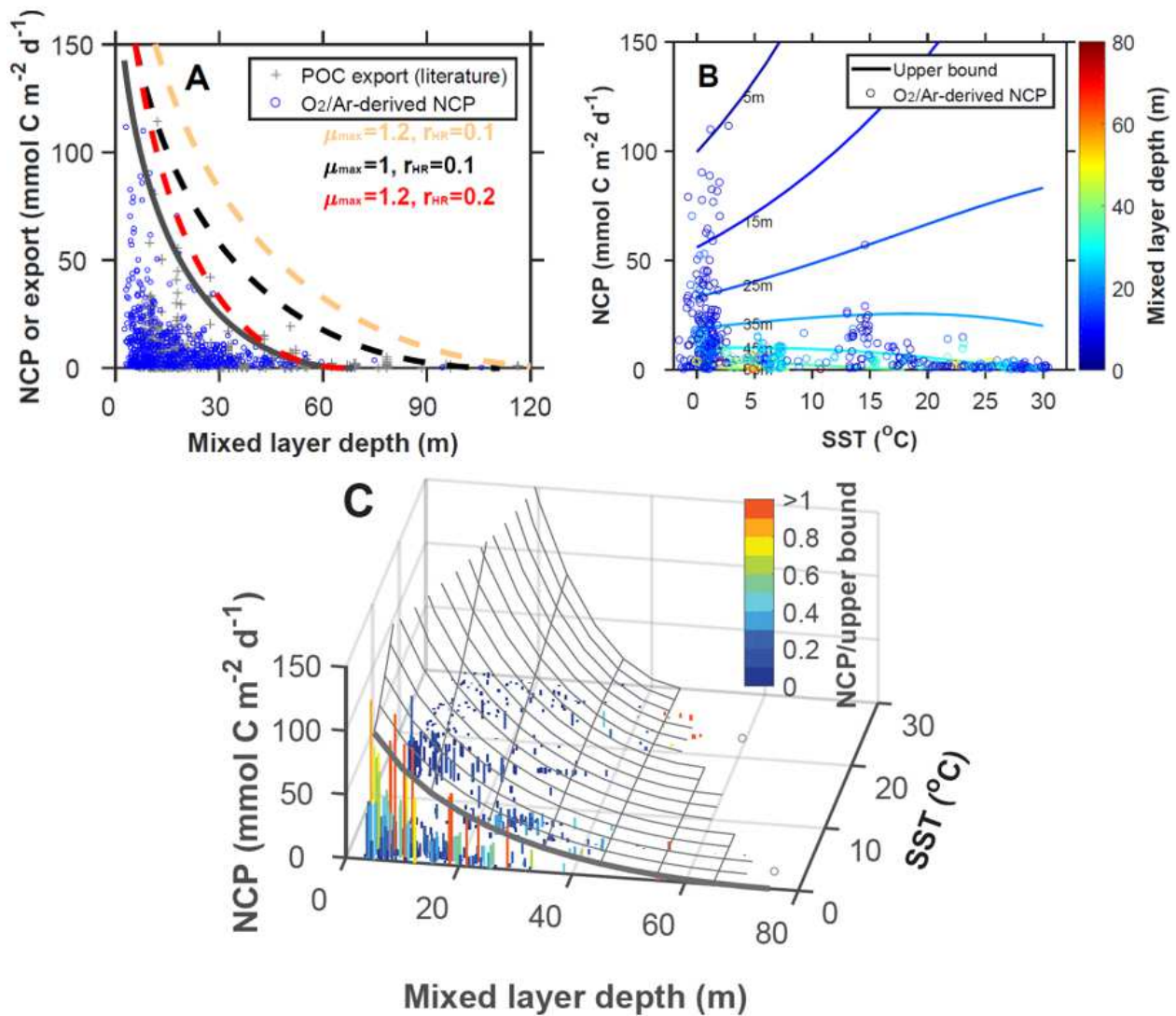


Figure 4. Envelope of the modeled upper bound on carbon export production compared to field observations as a function of mixed layer depth (MLD) and sea surface temperature (SST). (A) The thick gray line represents the upper bound fitted to the net community production (NCP) data. Dash-lines represent the upper bounds calculated using parameters available in the literature (Table 2). (B) NCP as a function of SST with isopleths of constant upper bounds color coded for MLD. NCP observations are color coded with MLD. (C) Surface representing the envelope of the modeled upper bound of carbon export production as a function of SST and MLD. Bars represent field observations color coded with the ratio of NCP to the upper bound.

Observations are based on ^{234}Th and sediment traps estimates of carbon export production and O_2/Ar -derived NCP. A stoichiometric ratio of $\text{O}_2/\text{C}=1.4$ was used to convert NCP from O_2 to C units (Laws, 1991). To account for the effect of PAR on export production, both MLD and carbon fluxes are normalized to $-\log(1 - I_m(0))$ (see equations (19) and (21)). The temperature dependence of r_{HR} was modeled as $r_{HR} = r_{HR}^0 \times e^{0.08 \times T}$.

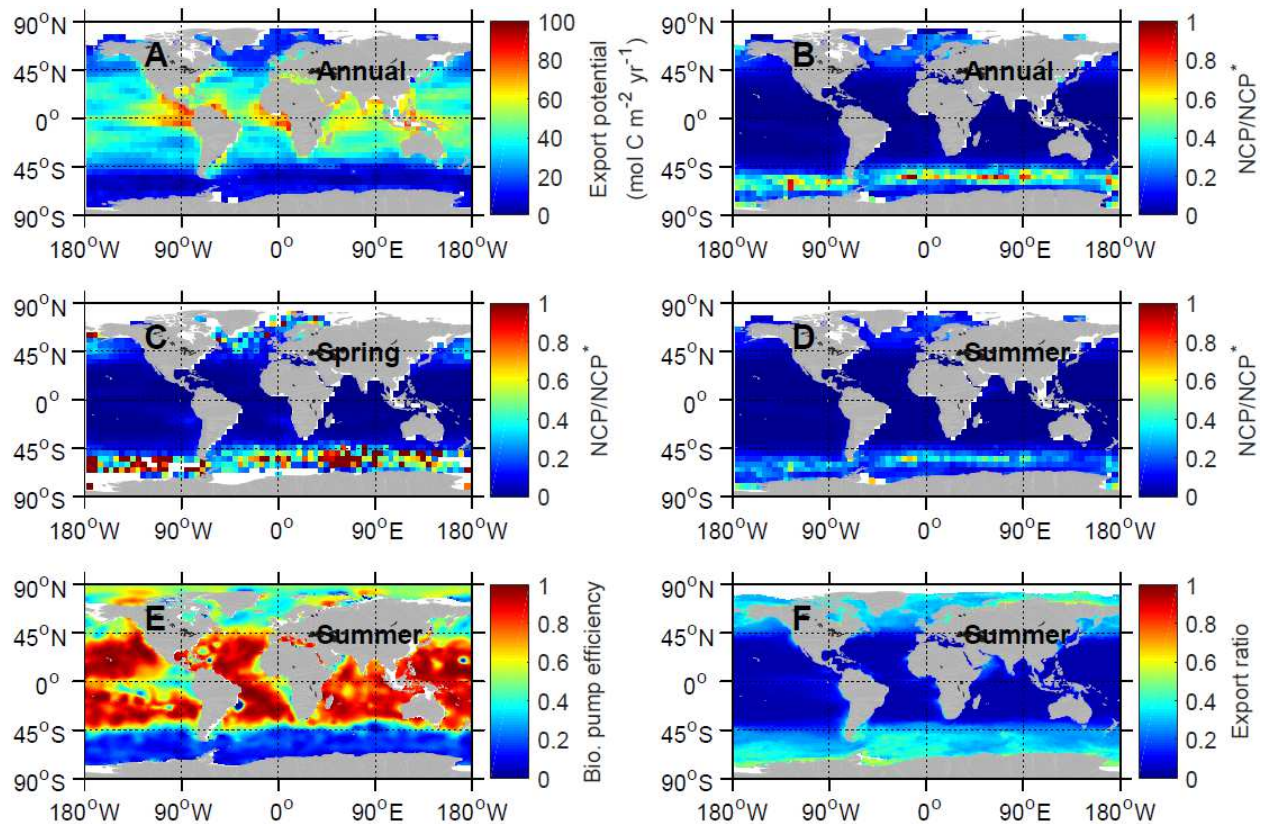


Figure 5. (A) Modeled upper bound on carbon export derived from equation (19), (B-D) ratios of satellite export production estimates to the upper bound on carbon export, (E) biological pump efficiency calculated as the difference in nutrient concentrations between surface and depth, normalized to nutrient concentrations at depth (Sarmiento and Gruber, 2006) (nitrate concentration from World Ocean Atlas (<https://www.nodc.noaa.gov/OC5/woa13/>)), and (F) export ratio derived from Dunne et al. (2005). Annual represents annually-integrated value. Spring and summer represent average value in spring and summer, respectively. In the northern hemisphere, spring and summer seasons are defined as March-May and June-August, respectively. In the southern hemisphere, spring and summer seasons are defined as September-November and December-February, respectively.

Table 1. Model symbols, abbreviations, and units

Symbol	Description	Units
MLD	Mixed layer depth	m
$MLD_{C^*_{max}}$	Maximum MLD corresponds to maximum achievable autotroph's biomass concentration	m
z	Depth	m
Z_c	Critical depth	m
Z_p	Compensation depth	m
GPP(0,z)	Gross primary production	mmol C m ⁻² d ⁻¹
NPP(z)	Net primary production at depth z	mmol C m ⁻³ d ⁻¹
NPP(0,z)	Net primary production above depth z	mmol C m ⁻² d ⁻¹
NCP(z)	Net community production at depth z	mmol C m ⁻³ d ⁻¹
NCP(0,z)	Net community production above depth z	mmol C m ⁻² d ⁻¹
HR(z)	Heterotrophic respiration at depth z	mmol C m ⁻³ d ⁻¹
HR(0,z)	Heterotrophic respiration above depth z	mmol C m ⁻² d ⁻¹
NCP^*	The maximum NCP for a given MLD (upper bound on carbon export)	mmol C m ⁻² d ⁻¹
NCP_B	NCP normalized to autotroph's biomass inventory in the mixed layer	d ⁻¹
ef	Export ratio	unitless
f_{pt}	Ratio of satellite export production estimates to the upper bound on carbon export	unitless
N	Nutrient concentration	mmol m ⁻³
k_m^N	Half-saturation constant for nutrient concentration	mmol m ⁻³
N_m	Nutrient effect on phytoplankton grow $N_m = \frac{N}{N+k_m^N}$	unitless
PAR	Photosynthetically active radiation	Einstein m ⁻² d ⁻¹
I_0	Photosynthetically active radiation just beneath water surface	Einstein m ⁻² d ⁻¹
$I(z)$	Photosynthetically active radiation at depth z	Einstein m ⁻² d ⁻¹
k_m^I	Half-saturation constant for irradiance	Einstein m ⁻² d ⁻¹
$I_m(z)$	Light effect on phytoplankton grow at depth z, $I_m(z) = \frac{I(z)}{I(z)+k_m^I} = \frac{I_0 \times e^{-K_I \times z}}{I_0 \times e^{-K_I \times z} + k_m^I}$	unitless
$I_m(0, z)$	Integrated light effect on phytoplankton grow above depth z, $I_m(0, z) = -\frac{1}{K_I} \times \ln\left(\frac{I_0 \times e^{-K_I \times z} + k_m^I}{I_0 + k_m^I}\right)$	unitless
PAR_{ML}	Average PAR in the mixed layer ($PAR_{ML} = \frac{1-e^{-K_I \times MLD}}{K_I \times MLD} \times I_0$)	Einstein m ⁻² d ⁻¹
μ	Phytoplankton growth rate	d ⁻¹
μ_{max}	Maximum phytoplankton growth rate	d ⁻¹

μ_{max}^0	Maximum phytoplankton growth rate for $T = 0$ °C	d^{-1}
r_{HR}	Heterotrophic respiration ratio	d^{-1}
r_{HR}^0	Heterotrophic respiration ratio for $T = 0$ °C	d^{-1}
K_I	Diffusion-Light attenuation coefficient ($K_I = K_I^w + K_I^{nw}$)	m^{-1}
K_I^w	Diffusion-Light attenuation coefficient due to water	m^{-1}
K_I^{nw}	Diffusion-Light attenuation coefficient due to optically active components	m^{-1}
k_c	Specific attenuation coefficient for irradiance	$m^2 \text{ mmol}^{-1}$
C	Phytoplankton biomass concentration	mmol m^{-3}
C^*	Phytoplankton biomass concentration that maximizes NCP	mmol m^{-3}
C_{max}^*	Maximum achievable autotroph's biomass concentration	mmol m^{-3}
POC	Particulate organic carbon	mmol m^{-3}
DOC	Dissolved organic carbon	mmol m^{-3}
CDOM	Colored dissolved organic matter	m^{-1}
NAP	Non-algal particles	mmol m^{-3}
T	Temperature	°C
P_t	Temperature dependence for phytoplankton grow rate	°C ⁻¹
B_t	Temperature dependence for heterotrophic respiration ratio	°C ⁻¹
CO ₂	Carbon dioxide	ppmv

Table 2. Value or range of values with references for the parameters used in the model.

Parameter	Range or value	Reference
K_I^w	<u>0.09</u>	<u>(Werdell and Bailey, 2005)</u>
k_c	<u>0.03</u>	<u>(Werdell and Bailey, 2005)</u>
Carbon to chlorophyll ratio	90	<u>(Arrigo et al., 2008)</u>
k_m^I	<u>4.1 Einstein m⁻² d⁻¹</u>	<u>(Behrenfeld and Falkowski, 1997)</u>
P_t	<u>0.0663</u>	<u>(Eppley, 1972)</u>
B_t	<u>0.08</u>	<u>(Rivkin and Legendre, 2001; López-Urrutia et al., 2006)</u>
μ_{max}	<u>1 d⁻¹, 1.2 d⁻¹</u>	<u>(Laws et al., 2000; Eppley, 1972)</u>
r_{HR}	<u>0.1 d⁻¹, 0.2 d⁻¹</u>	<u>(Laws et al., 2000; Mitchell et al., 1991)</u>

Supplementary for: **A mechanistic model of an upper bound on oceanic carbon export as a function of mixed layer depth and temperature**

Zuchuan Li*, Nicolas Cassar

Division of Earth and Ocean Sciences, Nicholas School of the Environment, Duke University, Durham, North Carolina, USA

* Corresponding to: zuchuan.li@duke.edu

1. Derivation of first and second derivatives of $NCP(0, MLD)$

To explore how $NCP(0, MLD)$ varies with C , we calculate its first and second derivatives with respect to C .

Based on equations (8-10):

$$\begin{aligned}
 & \frac{dNCP(0, MLD)}{dC} \\
 &= \frac{d \left\{ -N_m \times \mu_{max} \times \frac{\ln \left(\frac{I_0 \times e^{-K_I \times MLD} + k_m^I}{I_0 + k_m^I} \right) \times C}{K_I} \right\}}{dC} - \frac{d\{r_{HR} \times C \times MLD\}}{dC} \\
 &= -N_m \times \mu_{max} \\
 & \times \frac{\left\{ \ln \left(\frac{I_0 \times e^{-K_I \times MLD} + k_m^I}{I_0 + k_m^I} \right) - C \times \frac{I_0 + k_m^I}{I_0 \times e^{-K_I \times MLD} + k_m^I} \times \frac{I_0 \times e^{-K_I \times MLD}}{I_0 + k_m^I} \times k_c \times MLD \right\} \times K_I - k_c \times C \times \ln \left(\frac{I_0 \times e^{-K_I \times MLD} + k_m^I}{I_0 + k_m^I} \right)}{K_I^2} \\
 & - r_{HR} \times MLD \\
 &= -N_m \times \mu_{max} \times \frac{\{-K_I \times I_m(0, MLD) - C \times I_m(MLD) \times k_c \times MLD\} \times K_I + k_c \times C \times K_I \times I_m(0, MLD)}{K_I^2} - r_{HR} \times MLD \\
 &= N_m \times \mu_{max} \times \frac{K_I \times I_m(0, MLD) + k_c \times C \times I_m(MLD) \times MLD - k_c \times C \times I_m(0, MLD)}{K_I} - r_{HR} \times MLD \\
 &= N_m \times \mu_{max} \times \frac{K_I \times I_m(0, MLD) - k_c \times C \times I_m(0, MLD) + k_c \times C \times MLD \times I_m(MLD)}{K_I} - r_{HR} \times MLD \\
 &= N_m \times \mu_{max} \times \frac{K_I^W \times I_m(0, MLD) + k_c \times C \times MLD \times I_m(MLD)}{K_I^W + k_c \times C} - r_{HR} \times MLD \quad (S1)
 \end{aligned}$$

where $I_m(MLD) = \frac{I_0 \times e^{-K_I \times MLD}}{I_0 \times e^{-K_I \times MLD} + k_m^I}$.

Based on equation (S1), the second derivative of $NCP(0, MLD)$ in equation (8) with respect to C may be expressed as follows:

$$\frac{d^2 NCP(0, MLD)}{dC^2} = N_m \times \mu_{max} \times \left\{ \frac{dy}{dC} + \frac{dg}{dC} \right\} \quad (S2)$$

where $y = \frac{K_I^W \times I_m(0, MLD)}{K_I} = -\frac{K_I^W \times \ln \left(\frac{I_0 \times e^{-K_I \times MLD} + k_m^I}{I_0 + k_m^I} \right)}{K_I^2}$ and $g = \frac{k_c \times C \times MLD \times I_m(MLD)}{K_I}$.

$\frac{dy}{dC}$ and $\frac{dg}{dC}$ are derived as follows:

$$\begin{aligned}
\frac{dy}{dC} &= -K_I^w \times \frac{\frac{I_0 + k_m^I}{I_0 \times e^{-K_I \times MLD} + k_m^I} \times \frac{I_0 \times e^{-K_I \times MLD}}{I_0 + k_m^I} \times (-k_c \times MLD) \times K_I^2 - \ln\left(\frac{I_0 \times e^{-K_I \times MLD} + k_m^I}{I_0 + k_m^I}\right) \times 2 \times K_I \times k_c}{K_I^4} \\
&= -K_I^w \times \frac{-I_m(MLD) \times MLD \times K_I^2 + I_m(0, MLD) \times 2 \times K_I^2}{K_I^4} \times k_c \\
&= K_I^w \times \frac{I_m(MLD) \times MLD - 2 \times I_m(0, MLD)}{K_I^2} \times k_c \quad (S3)
\end{aligned}$$

$$\begin{aligned}
\frac{dg}{dC} &= \frac{-k_c \times C \times MLD \times I_m(MLD) \times k_c + k_c \times MLD \times I_m(MLD) \times K_I}{K_I^2} \\
&+ \frac{k_c \times C \times MLD \times \frac{I_0 \times e^{-K_I \times MLD} \times (-k_c \times MLD) \times \{I_0 \times e^{-K_I \times MLD} + k_m^I\} - I_0 \times e^{-K_I \times MLD} \times I_0 \times e^{-K_I \times MLD} \times (-k_c \times MLD)}{\{I_0 \times e^{-K_I \times MLD} + k_m^I\}^2} \times K_I}{K_I^2} \\
&= \frac{k_c \times MLD \times I_m(MLD) \times K_I + k_c \times C \times MLD \times \frac{I_0 \times e^{-K_I \times MLD} \times (-k_c \times MLD) \times k_m^I}{\{I_0 \times e^{-K_I \times MLD} + k_m^I\}^2} \times K_I - k_c^2 \times C \times MLD \times I_m(MLD)}{K_I^2} \\
&= \frac{k_c \times MLD \times I_m(MLD) \times K_I + k_c \times C \times MLD \times \frac{I_m(MLD)^2 \times (-k_c \times MLD) \times k_m^I}{I_0 \times e^{-K_I \times MLD}} \times K_I - k_c^2 \times C \times MLD \times I_m(MLD)}{K_I^2} \\
&= \frac{MLD \times I_m(MLD) \times K_I + k_c \times C \times MLD \times \frac{-I_m(MLD)^2 \times MLD \times k_m^I}{I_0 \times e^{-K_I \times MLD}} \times K_I - k_c \times C \times MLD \times I_m(MLD)}{K_I^2} \times k_c \\
&= \frac{MLD \times I_m(MLD) \times K_I - k_c \times C \times MLD \times I_m(MLD)}{K_I^2} \times k_c - \frac{k_c \times C \times MLD \times \frac{I_m(MLD)^2 \times MLD \times k_m^I}{I_0 \times e^{-K_I \times MLD}} \times K_I}{K_I^2} \times k_c \\
&= \frac{MLD \times I_m(MLD) \times K_I^w}{K_I^2} \times k_c - \frac{MLD^2 \times C \times I_m(MLD)^2 \times k_m^I}{K_I \times I_0 \times e^{-K_I \times MLD}} \times k_c^2 \quad (S4)
\end{aligned}$$

Substituting equations (S3-S4) into equation (S2) yields:

$$\begin{aligned}
\frac{d^2NCP(0, MLD)}{dC^2} &= N_m \times \mu_{max} \times \left\{ K_I^w \times \frac{I_m(MLD) \times MLD - 2 \times I_m(0, MLD)}{K_I^2} \times k_c + \frac{MLD \times I_m(MLD) \times K_I^w}{K_I^2} \times k_c - \frac{MLD^2 \times C \times I_m(MLD)^2 \times k_m^I}{K_I \times I_0 \times e^{-K_I \times MLD}} \right. \\
&\quad \left. \times k_c^2 \right\} \\
&= N_m \times \frac{\mu_{max}}{K_I} \times k_c \times \left\{ \frac{2 \times K_I^w}{K_I} \times (I_m(MLD) \times MLD - I_m(0, MLD)) - \frac{MLD^2 \times C \times I_m(MLD)^2 \times k_m^I}{I_0 \times e^{-K_I \times MLD}} \times k_c \right\} \quad (S5)
\end{aligned}$$

2. NCP upper bound for shallow MLD

When $0 \leq MLD < MLD_{C_{max}^*}$ and $MLD \rightarrow 0$, $1 - \exp(-K_I \times MLD)$ in equation (15) can be approximated using a second order of Taylor expansion:

$$1 - \exp(-K_I \times MLD) \approx K_I \times MLD - \frac{1}{2} \times (K_I \times MLD)^2 \quad (S6)$$

From equation (S6), we may approximate equation (15):

$$NCP(0, MLD) = C \times MLD \times \left(-\frac{1}{2} \times K_I \times MLD \times \mu^* + \mu^* - r_{HR} \right) \quad (S7)$$

where the first derivative of equation (S7) with respect to C is:

$$\frac{dNCP(0, MLD)}{dC} = MLD \times \left(-K_I^{nw} \times MLD \times \mu^* - \frac{1}{2} \times K_I^w \times MLD \times \mu^* + \mu^* - r_{HR} \right) \quad (S8)$$

when $0 \leq MLD < MLD_{C_{max}^*}$, K_I^{nw} should satisfy $K_I^{nw} \leq k_c \times C_{max}^* < -\frac{1}{2} \times K_I^w + \frac{\mu^* - r_{HR}}{\mu^*} \times \frac{1}{MLD}$, and equation (S8) should be greater than 0. $NCP(0, MLD)$ thus increases with C in the range of $0 \leq MLD < MLD_{C_{max}^*}$, with an upper bound obtained at C_{max}^* :

$$NCP^* = \mu^* \times C_{max}^* \times MLD \times \left(-\frac{1}{2} \times (k_c \times C_{max}^* + K_I^w) \times MLD + \frac{\mu^* - r_{HR}}{\mu^*} \right) \quad (S9)$$

Over this range, Equation (S9) states that NCP^* increases with MLD , and as expected is nil when MLD equals 0.

3. An upper bound on export ratio

The export ratio ef (equation (24)) is written as follows:

$$ef = \frac{NCP(0, MLD)}{NPP(0, MLD)} = 1 - \frac{K_I \times MLD}{-\ln\left(\frac{I_0 \times e^{-K_I \times MLD} + k_m^I}{I_0 + k_m^I}\right)} \times \frac{1}{N_m} \times \frac{r_{HR}}{\mu_{max}} \quad (S10)$$

where $MLD_{\text{opt}} = \frac{K_I \times MLD}{1 - e^{-K_I \times MLD}}$. The first derivative of ef with respect to $K_I \times MLD$ is expressed as:

$$\frac{\partial ef}{\partial C} = - \left(1 - \frac{MLD \times I_m(MLD)}{I_m(0, MLD)} \right) \times \frac{1}{K_I} \times k_c \times (1 - ef) \quad (S11)$$

Because $e^{\frac{K_I \times MLD}{1 - e^{-K_I \times MLD}}} > 1 + K_I \times MLD$ for $K_I \times MLD > 0$, According to the inequality in equation (13), $\frac{\partial ef}{\partial C}$ in

equation (S11) must be less than 0. Therefore, minimum of ef approximates to 1 when

$K_I \times MLD \rightarrow 0$ ($ef = 1 - \frac{1}{I_m(0)} \times \frac{1}{N_m} \times \frac{r_{HR}}{\mu_{max}}$). Considering that, the minimum values for the terms

$\frac{1}{N_m}$ and $\frac{1}{I_m(0)}$ in equation (S10) have the minimum of α . Therefore, ef is maximized in the maximum of

equation (S10) ~~is has with the maximum of~~ $ef^* = 1 - \frac{r_{HR}}{\mu_{max}} = 1 - \alpha \times e^{(B_T - P_T) \times T}$, where α represents an

constant, $B_T = 0.11$ and $P_T = 0.0633$ for the equation (5) of Cael and Follows (2016).

4. Dataset

To test the performance of our upper bound model, we compiled observations of net community production (Table S1) and carbon export in the world's oceans.

4.1 O₂/Ar Net Community Production

The O₂/Ar method estimates NCP through a mass balance of biological O₂ in the mixed layer. Because Ar and O₂ have similar temperature dependencies and solubilities (Craig and Hayward, 1987), the saturation state of their ratio can partition oxygen concentration due to physical ($[O_2]_{phys}$) and biological processes ($[O_2]_{biol}$) (Cassar et al., 2011):

$$[O_2]_{biol} = [O_2] - [O_2]_{phys} \approx [O_2] - \frac{[Ar]}{[Ar]_{sat}} [O_2]_{sat} = \frac{[Ar]}{[Ar]_{sat}} [O_2]_{sat} \Delta(O_2/Ar) \quad (S12)$$

where $\Delta(O_2/Ar) = \left[\frac{([O_2]/[Ar])}{([O_2]/[Ar])_{sat}} - 1 \right]$ is the biological O₂ supersaturation. When ignoring vertical mixing and

lateral advection, we can write the mass balance for $[O_2]_{biol}$ in the mixed layer as follows (Cassar et al., 2011):

$$MLD \frac{d[O_2]_{biol}}{dt} = NCP - k_{O_2} \frac{[Ar]}{[Ar]_{sat}} [O_2]_{sat} \Delta(O_2/Ar) \quad (S13)$$

where k_{O_2} is the gas exchange velocity for O₂. At steady state (i.e., $\frac{d[O_2]_{biol}}{dt} = 0$), equation (S13) reduces to

(Cassar et al., 2011; Reuer et al., 2007):

$$NCP = k_{O_2} [O_2]_{sat} \Delta(O_2/Ar) \quad (S14)$$

where $\frac{[Ar]}{[Ar]_{sat}}$ in equation (S13) is assumed to equal 1, which introduces an error of up to a couple percent in NCP estimates under most conditions (Cassar et al., 2011; Eveleth et al., 2014).

To derive NCP using equation (S14), we calculate k_{O_2} using daily NCEP wind speeds, MLD, the parameterization of Wanninkhof (1992), and a weighting technique to account for wind speed history following

(Reuer et al., 2007). Uncertainties and biases in O₂/Ar NCP estimates can be found in previous studies (Bender et al., 2011; Cassar et al., 2014; Jonsson et al., 2013).

Table S1. O₂/Ar measurements included in this study.

Citation	Cruise	Start date	End date	Location
(Reuer et al., 2007)	A0103	10/30/2001	12/10/2001	South of Australia
	SOFEXR	01/07/2002	02/12/2002	South of New Zealand
	SOFEXM	01/20/2002	02/24/2002	South of New Zealand
	NBP0305	10/28/2003	11/13/2003	South of New Zealand
	ANTXXI/2	11/18/2003	01/15/2004	South of South Africa
	NBP0305A	12/20/2003	12/29/2003	South of New Zealand
(Cassar et al., 2007)	AA2006	12/03/2005	02/09/2006	South of Australia
(Juranek et al., 2010)	AMT16	05/22/2005	06/28/2005	Atlantic
	AMT17	10/18/2005	11/25/2005	Atlantic
(Stanley et al., 2010)	EUC-Fe	07/19/2006	08/31/2006	Equatorial Pacific
(Tortell et al., 2011)	CORSACS II	11/03/2006	12/11/2006	South of New Zealand
(Cassar et al., 2011)	SAZ-SENSE	01/19/2007	02/19/2007	South of Australia
(Huang et al., 2012)	LMG0801	01/07/2008	01/29/2008	Drake Passage
(Hamme et al., 2012)	GASEX	03/02/2008	04/11/2008	South of Atlantic
(Martin et al., 2013)	LOHAFEX	01/26/2009	03/06/2009	South of Atlantic
(Shadwick et al., 2015)	AA1203	01/08/2012	02/10/2012	South of Australia
(Eveleth et al., 2016)	LMG1201	12/30/2011	02/07/2012	Drake Passage
	LMG1301	01/05/2013	02/03/2013	Drake Passage
	LMG1401	01/01/2014	02/01/2014	Drake Passage
(Huang et al., unpublished)	LMG0901	01/06/2009	02/01/2009	Drake Passage
	LMG1001	01/01/2010	02/07/2010	Drake Passage
	LMG1101	01/02/2011	02/06/2011	Drake Passage

4.2 Sediment trap and ²³⁴Thorium POC export production

We also compared *NCP** to sediment-trap and ²³⁴Th-derived POC export production estimates from the dataset recently compiled by Mouw et al. (2016). These observations were adjusted to reflect a flux at the base of the mixed layer using the Martin curve with $b = -0.86$ (Martin et al., 1987). Monthly climatological MLD were used.

4.3 Mixed layer depth

We derived MLD using Argo temperature-salinity profiling floats which were downloaded from <http://www.usgodae.org/>. As real-time data (after 2008) have not been thoroughly checked, we only used profiles with temperature, salinity, and pressure with a quality flag of '1' ('good data') or '2' ('probably good data'). To improve coverage, we also used the temperature and salinity profiles obtained by CTD casts in the World Ocean Database. These profiles were downloaded from the National Oceanographic Data Center (NODC) <https://www.nodc.noaa.gov/access/index.html>.

MLD is estimated as the depth at which the potential density (σ_θ) exceeds a near-surface reference value at 10 m depth by $\Delta\sigma_\theta = 0.03 \text{ kg m}^{-3}$ (de Boyer Montegut et al., 2004; Dong et al., 2008). Estimates were averaged to daily $5^\circ \times 5^\circ$ grids, from which monthly climatologies were calculated (Figure S1).

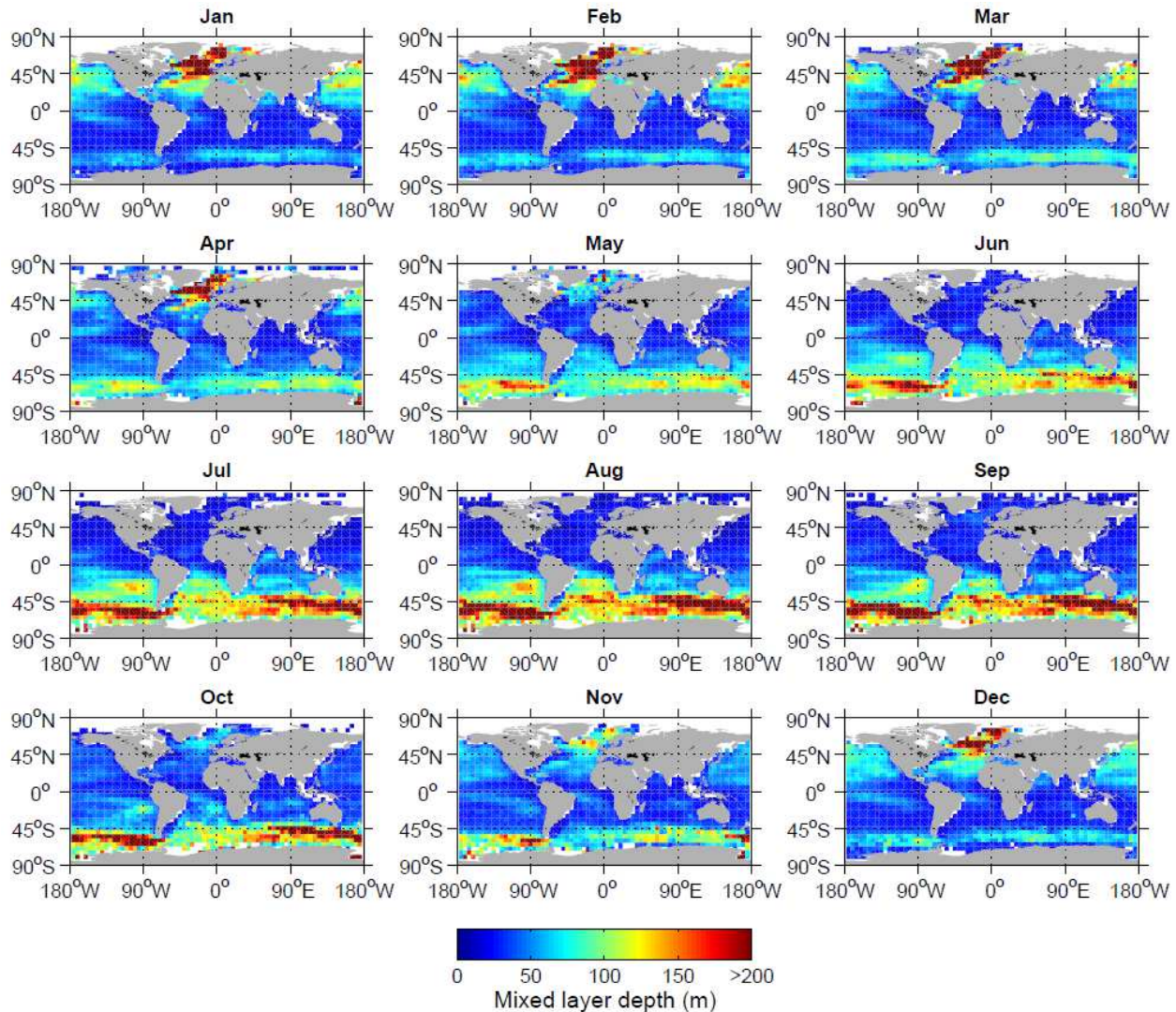


Figure S1. Climatology of monthly mixed layer depth.

4.4 Satellite properties

To derive a global distribution of NCP^* , we used monthly SST and PAR climatologies calculated based on MODIS-Aqua observations from 2002-2015 with a spatial resolution of $0.083^\circ \times 0.083^\circ$ (downloaded from NASA's ocean color website (<http://oceancolor.gsfc.nasa.gov/cms/>)). We compared NCP^* to monthly and annual NCP climatologies as simulated by the algorithms developed by Li and Cassar (2016). This NCP dataset

represents the average of 11 satellite algorithms of export production for observations from 1997 to 2010 (Figure S2). More details can be found in Li and Cassar (2016).

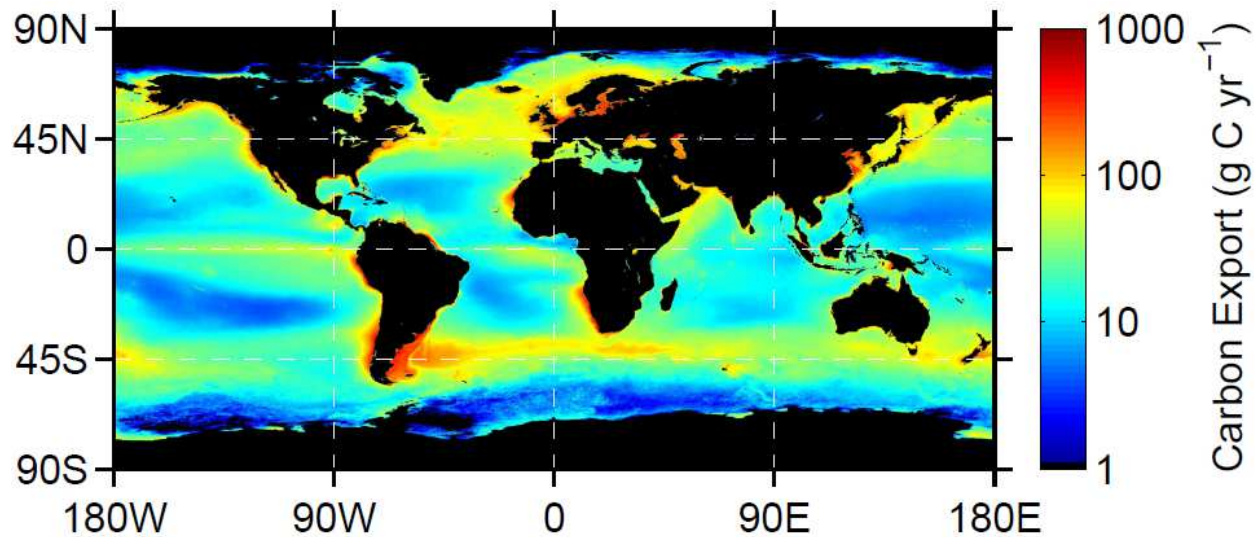


Figure 2S. Average annual export production derived using 11 algorithms (see Li and Cassar (2016)).

4.5. Diffusion attenuation coefficient for photosynthetically active radiation

Constants k_c and K_I^w in equation (10) were derived using the NOMAD dataset (Werdell and Bailey, 2005), which includes chlorophyll a concentration and K_I (Figure S3). NOMAD was downloaded from <https://seabass.gsfc.nasa.gov/wiki/NOMAD>. The regression in Figure S3 was converted to equation (10) using a carbon to chlorophyll ratio of 90 (Arrigo et al., 2008).

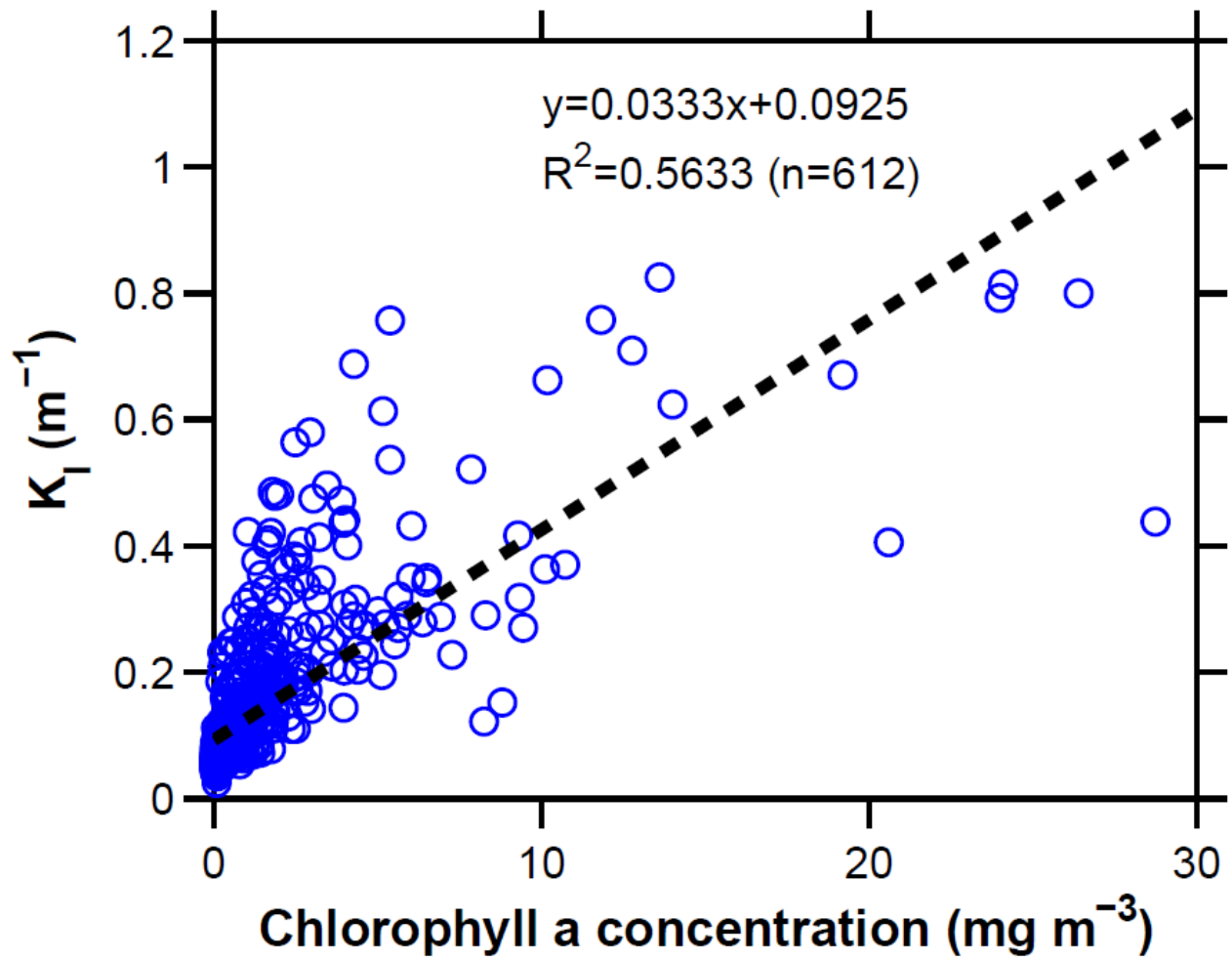


Figure S3. Attenuation coefficient for photosynthetically active radiation (PAR) as a function of chlorophyll a concentration based on the NOMAD dataset.

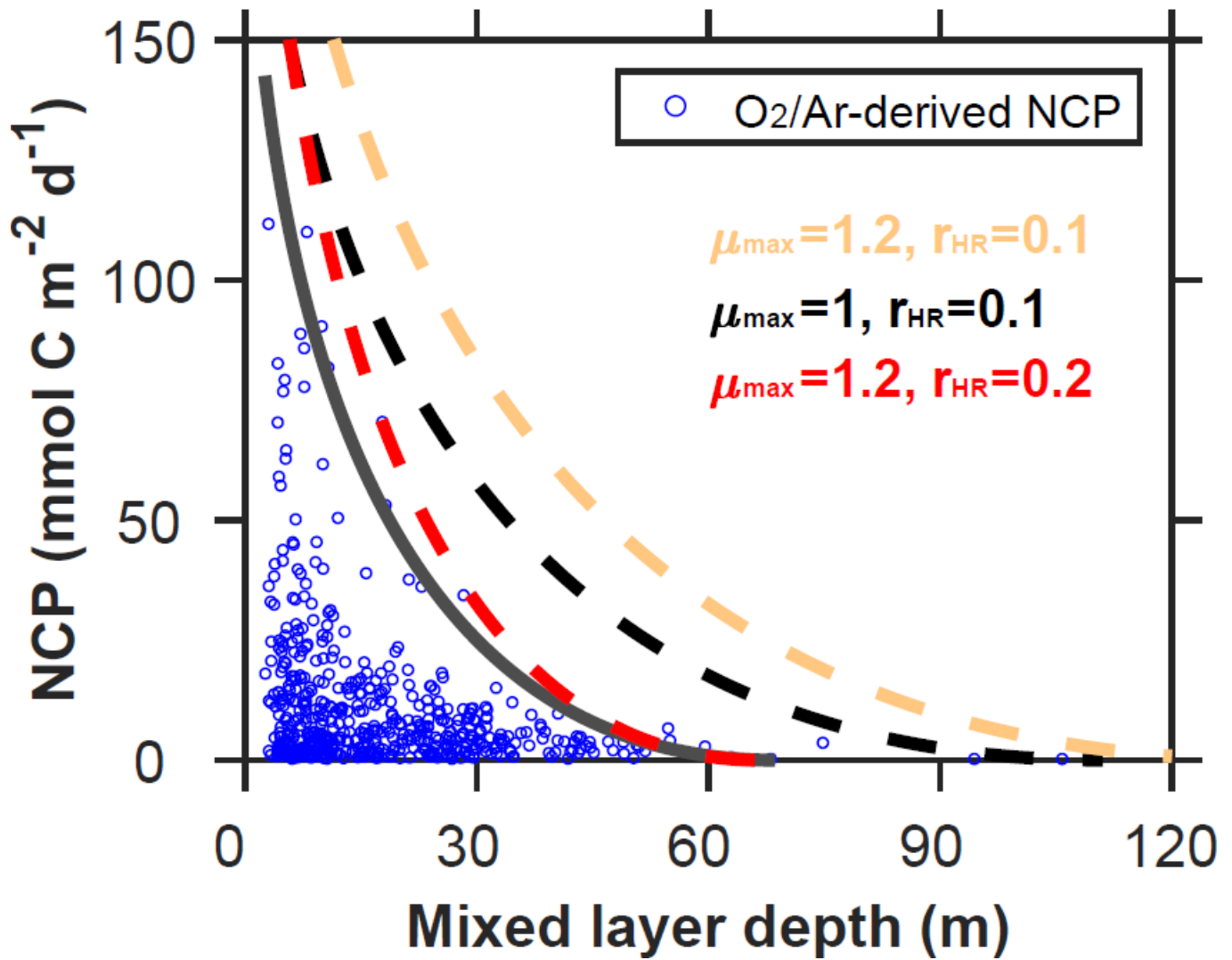


Figure S4. Modeled upper bound on carbon export production compared to field observations as a function of mixed layer depth (MLD). Observations are based on O₂/Ar-derived net community production (NCP). To account for the effect of photosynthetically active radiation (PAR) on export production, both MLD and carbon fluxes are normalized to $-\log(1 - I_m(0))$ (see equations (19) and (21)). The thick gray line represents the upper bound fitted to the NCP data. Dash-lines represent the upper bounds calculated using parameters available in the literature (Table 2). A stoichiometric ratio of O₂/C=1.4 was used to convert NCP from O₂ to C units (Laws, 1991).

References

- Arrigo, K. R., van Dijken, G. L., and Bushinsky, S.: Primary production in the Southern Ocean, 1997-2006, *J. Geophys. Res.*, 113, doi:10.1029/2007JC004551, 2008.
- Bender, M. L., Kinter, S., Cassar, N., and Wanninkhof, R.: Evaluating gas transfer velocity parameterizations using upper ocean radon distributions, *J. Geophys. Res.*, 116, doi:10.1029/2009JC005805, 2011.
- Cael, B. B. and Follows, M. J.: On the temperature dependence of oceanic export efficiency, *Geophys. Res. Lett.*, 43, 5170-5175, doi:10.1002/2016GL068877, 2016.
- Cassar, N., Nevison, C. D., and Manizza, M.: Correcting oceanic O₂/Ar-net community production estimates for vertical mixing using N₂O observations, *Geophys. Res. Lett.*, 41, 8961-8970, doi:10.1002/2014GL062040, 2014.
- Cassar, N., Bender, M. L., Barnett, B. A., Fan, S., Moxim, W. J., Levy, H., and Tilbrook, B.: The Southern Ocean biological response to aeolian iron deposition, *Science*, 317, 1067-1070, doi:10.1126/science.1144602, 2007.
- Cassar, N., DiFiore, P. J., Barnett, B. A., Bender, M. L., Bowie, A. R., Tilbrook, B., Petrou, K., Westwood, K. J., Wright, S. W., and Lefevre, D.: The influence of iron and light on net community production in the Subantarctic and Polar Frontal Zones, *Biogeosciences*, 8, 227-237, doi:10.5194/bg-8-227-2011, 2011.
- Craig, H. and Hayward, T.: Oxygen supersaturation in the ocean: Biological versus physical contributions, *Science*, 235, 199-202, doi:10.1126/science.235.4785.199, 1987.
- de Boyer Montegut, C., Madec, G., Fischer, A. S., Lazar, A., and Iudicone, D.: Mixed layer depth over the global ocean: An examination of profile data and a profile-based climatology, *Journal of Geophysical Research-Oceans*, 109, doi:10.1029/2004JC002378, 2004.
- Dong, S., J. Sprintall, Gille, S. T., and Talley, L.: Southern Ocean mixed-layer depth from Argo float profiles, *Journal of Geophysical Research-Oceans*, 113, doi:10.1029/2006JC004051, 2008.
- Eveleth, R., Timmermans, M. L., and Cassar, N.: Physical and biological controls on oxygen saturation variability in the upper Arctic Ocean, *Journal of Geophysical Research-Oceans*, 119, 7420-7432, doi:10.1002/2014JC009816, 2014.
- Eveleth, R., Cassar, N., Sherrell, R. M., Ducklow, H., Meredith, M., Venables, H., Lin, Y., and Li, Z.: Ice melt influence on summertime net community production along the Western Antarctic Peninsula, *Deep Sea Research Part II.*, 139, 89-102, doi:10.1016/j.dsr2.2016.07.016, 2017.
- Hamme, R. C., Cassar, N., Lance, V. P., Vaillancourt, R. D., Bender, M. L., Strutton, P. G., Moore, T. S., DeGrandpre, M. D., Sabine, C. L., Ho, D. T., and Hargreaves, B. R.: Dissolved O₂/Ar and other methods reveal rapid changes in productivity during a Lagrangian experiment in the Southern Ocean, *Journal of Geophysical Research-Oceans*, 117, doi:10.1029/2011JC007046, 2012.

- Huang, K., Ducklow, H., Vernet, M., Cassar, N., and Bender, M. L.: Export production and its regulating factors in the West Antarctica Peninsula region of the Southern Ocean, *Global Biogeochem Cy*, 26, doi:10.1029/2010GB004028, 2012.
- Jonsson, B. F., Doney, S. C., Dunne, J. P., and Bender, M. L.: Evaluation of the Southern Ocean O₂/Ar-based NCP estimates in a model framework, *Journal of geophysical Research*, 118, 385-399, doi:10.1002/jgrg.20032, 2013.
- Juranek, L. W., Hamme, R. C., Kaiser, J., Wanninkhof, R., and Quay, P. D.: Evidence of O₂ consumption in underway seawater lines: Implications for air-sea O₂ and CO₂ fluxes, *Geophys Res Lett*, 37, doi:10.1029/2009GL040423, 2010.
- Li, Z. and Cassar, N.: Satellite estimates of net community production based on O₂/Ar observations and comparison to other estimates, *Global Biogeochem Cy*, 30, 735-752, doi:10.1002/2015GB005314, 2016.
- Martin, J. H., Knauer, G. A., Karl, D. M., and Broenkow, W. W.: VERTEX: Carbon Cycling in the Northeast Pacific, *Deep Sea Research Part A*, 34, 267-285, doi:10.1016/0198-0149(87)90086-0, 1987.
- Martin, P., van der Loeff, M. R., Carssar, N., Vandromme, P., d'Ovidio, F., Stemann, L., Rengarajan, R., Soares, M., González, H. E., Ebersbach, F., Lampitt, R. S., Sanders, R., Barnett, B. A., Smetacek, V., and Naqvi, S. W. A.: Iron fertilization enhanced net community production but not downward particle flux during the Southern Ocean iron fertilization experiment LOHAFEX, *Global Biogeochem Cy*, 27, 871-881, doi:10.1002/gbc.20077, 2013.
- Mouw, C. B., Barnett, A., McKinley, G. A., Gloege, L., and Pilcher, D.: Global ocean particulate organic carbon flux merged with satellite parameters, *Earth System Science Data*, 8, 531-541, doi:10.5194/essd-8-531-2016, 2016.
- Reuer, M. K., Barnett, B. A., Bender, M. L., Falkowski, P. G., and Hendricks, M. B.: New estimates of Southern Ocean biological production rates from O₂/Ar ratios and the triple isotope composition of O₂, *Deep Sea Research Part I*, 54, 951-974, doi:10.1016/j.dsr.2007.02.007, 2007.
- Shadwick, E. H., Tilbrook, B., Cassar, N., Trull, T. W., and Rintoul, S. R.: Summertime physical and biological controls on O₂ and CO₂ in the Australian Sector of the Southern Ocean, *J Marine Syst*, 147, 21-28, doi:10.1016/j.jmarsys.2013.12.008, 2015.
- Stanley, R. H. R., Kirkpatrick, J. B., Cassar, N., Barnett, B. A., and Bender, M. L.: Net community production and gross primary production rates in the western equatorial Pacific, *Global Biogeochem Cy*, 24, doi:10.1029/2009GB003651, 2010.
- Tortell, P. D., Gueguen, C., Long, M. C., Payne, C. D., Lee, P., and DiTullio, G. R.: Spatial variability and temporal dynamics of surface water pCO₂, ΔO₂/Ar and dimethylsulfide in the Ross Sea, Antarctica, *Deep Sea Research Part I*, 58, 241-259, doi:10.1016/j.dsr.2010.12.006, 2011.
- Wanninkhof, R.: Relationship between wind speed and gas exchange over the Ocean, *Journal of Geophysical Research-Oceans*, 97, 7373-7382, doi:10.1029/92JC00188, 1992.

Werdell, P. J. and Bailey, S. W.: An improved in-situ bio-optical data set for ocean color algorithm development and satellite data product validation, *Remote Sensing of Environment*, 98, 122-140, doi:10.1016/j.rse.2005.07.001, 2005.